PHASE TRANSITIONS IN COLLOIDAL SUSPENSIONS OF VIRUS PARTICLES

SETH FRADEN
Martin Fisher School of Physics
Brandeis University
Waltham, Massachusetts USA

1. Introduction

Colloidal liquid crystals are a useful experimental system for studying fundamental aspects of liquid crystal ordering, because the time, energy, and size scales involved allow one to interact with the system with laboratory scale probes and forces, in a way that is not possible in small molecule systems. In the colloidal systems, liquid crystalline ordering arises from simple particle shape and excluded volume effects, rather than more complex interactions that occur in molecular systems involving van der Waals attractions, dipolar effects, and more complicated molecular interactions. The study of hard rod systems has recently been a subject of intensive theoretical investigation [1, 2, 3] prompted by a series of remarkable computer simulations [4, 5, 6, 7]. For comparing this body of theoretical work to a real physical system, solutions of virus particles have provided the only suitable experimental tests [8, 9, 10]. These studies have implications for all liquid crystals, because the symmetry and the nature of the ordered phases being studied are universal to a wide range of systems, including low molecular weight thermotropics and polymer liquid crystals. In this chapter we will discuss experiments exploring the liquid crystalline properties of colloidal suspensions of virus particles. Since an article summarizing TMV research at Brandeis was published recently [11], we will focus on studies not reviewed previously. A second review article on TMV research by Wetter [12] is especially recommended for its abundance of splendid photographs.

Our goal is to understand liquid crystal behavior on three different length scales; microscopic, mesoscopic, and macroscopic. On the microscopic scale we seek to determine the interparticle potential, which gener-

ally has both repulsive and attractive components. The mesoscopic scale is concerned with interparticle spatial, angular, and temporal correlations, and on the macroscopic scale we measure visco-elastic constants and explain a wide variety of phenomena treating the liquid crystal as a continuum visco-elastic medium. Equally importantly we wish to understand the interconnections between these length scales and finally seek a unified theoretical understanding of phenomena on all three scales.

The microscopic interparticle interactions influence properties at larger length scales, and from the studies of simple fluids, such as liquid argon, it has been shown that phase behavior and interparticle correlations are dominated by steric repulsion, with attractive forces playing a secondary role [13]. By isolating the repulsive interaction and studying model hard sphere systems, computer simulations, theory, and experiments on hard sphere colloids have contributed to our understanding of liquids and solids. The most notable conceptual advance being the realization that two-phase coexistence between a liquid and a crystal occurs at densities far below close packing in hard sphere systems. This is an example of an entropy driven phase transition where the seemingly higher ordered crystalline phase has greater entropy than the disordered liquid [14, 15, 16].

The idea that steric interactions dominate phase behavior of spherical molecules has been extended to liquid crystals by computer simulations of hard rods which exhibit a nematic - smectic (N - Sm) transition [4, 5, 6, 7]. Previously it was thought that specific attractive potentials were needed to produce a N - Sm transition. However, experimentally there are no liquid crystal forming anisotropic small molecules equivalent to argon, nor are there yet hard rod colloids similar to the hard sphere colloids (see the lectures of H. Lekkerkerker in this volume). Instead, we study charged particles interacting with a screened coulomb potential, which like the hard particle potential is short ranged and repulsive.

The rod shaped virus particles, Tobacco Mosaic Virus (TMV) and semi-flexible bacteriophages fd and pf1 remain unique experimental systems because they are the only colloidal suspensions of particles whose interactions are predominately repulsive, which with increasing concentration form isotropic, nematic (TMV and pf1) or cholesteric (fd), and smectic liquid crystals. In the isotropic phase both interparticle angular and spatial correlations are short ranged while in the nematic the long axes of the rods are parallel (long range angular correlations), but the center of masses have liquid-like short range correlations. In smectic suspensions the rods are also parallel, but rod ends are in register forming individual layers with liquid like order in each layer. Additionally, the rigid TMV particle has a colloidal crystalline phase where the aligned particles have their centers of mass located on a crystalline lattice and partially dried oriented fibers of
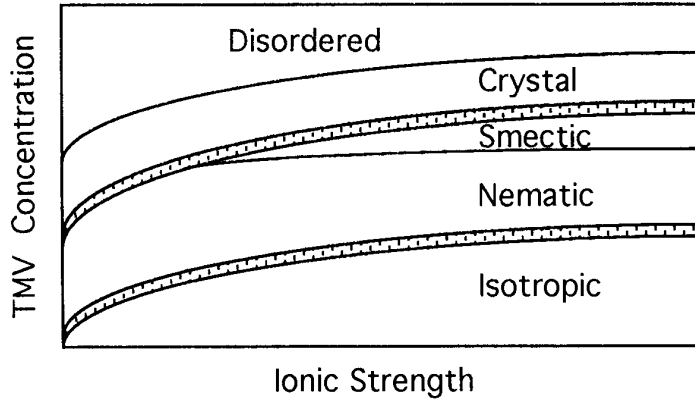
Figure 1. Tentative phase diagram of TMV as a function of ionic strength. At high ionic strengths the sequence isotropic, nematic, smectic, colloidal crystal, and disordered is observed with increasing concentration, while at low ionic strength there appears to be a direct transition from the nematic to the colloidal crystalline phase. The phase transitions are first order, except the nematic - smectic, which is second order. The nature of the disordered region is not understood in either TMV or fd.

fd, pf1, and TMV exhibit hexagonal columnar order [17, 18] with hexagonal packing of the viruses in the plane perpendicular to the particle axis (director) and short range correlations parallel to the director. However, it is not clear if the observations of columnar order have occurred in monodisperse samples, or in ones at equilibrium.

At high concentrations, both fd and TMV become somewhat disordered. Long range orientational order remains (the samples are birefringent), but long range spatial order vanishes (Bragg scattering disappears). The phase diagram is also a function of ionic strength since the range of the screened coulomb repulsion decreases with increasing ionic strength, which lowers the effective diameter of the particle. The phase diagrams of fd and TMV are schematically shown in Figures (1) and (2).

2. Physical properties of virus

The unique attribute of using virus particles as an experimental system for investigating liquid crystal behavior is that Nature has designed the viruses to be identical in structure, which gives rise to the same physical parameters such as mass, length, diameter, as well as charge density. Such a high degree of monodispersity is not currently obtainable using synthetic
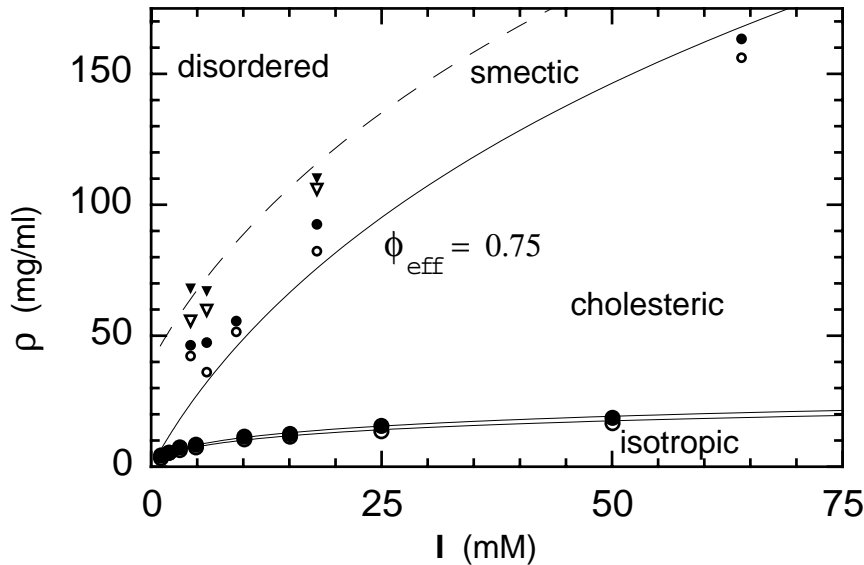
Figure 2. fd shows a sequence of isotropic (I), cholesteric (C), smectic (S), and disordered with increasing concentration. Both the I-C and C-S transitions are first order. The nature of the disordered region is not understood in either TMV or fd. The solid line along the C - S boundary corresponds to a constant effective volume fraction of $\phi = 0.75$ discussed in section (9). The open circles and triangles correspond to the highest measured concentrations of the cholesteric and smectic phases, respectively while the solid triangles and circles correspond to the lowest measured concentrations of the disordered and smectic phases, respectively.

chemical methods.

Viewed at low resolution in an electron microscope, TMV appears as a rigid rod of length $L = 300$ nm and diameter $D = 18$ nm [19] and light scattering studies have failed to detect any flexibility [20, 21]. TMV is composed of 2130 identical protein subunits arranged in a helix composed of 16 and 2/3 units per turn of the helix, wound about a hollow, water-filled center of 4 nm diameter. The units form a helical grooved outer surface resembling a finely threaded screw with the outer groove diameter 18 nm and the inner 16 nm. In addition to the protein, TMV contains a single strand of RNA running the entire length of the virus in a slot in the protein with three bases per protein subunit. TMV is a polyelectrolyte with an isoelectric point of about 3.5 and at pH 7 is negatively charged with a linear charge density of 10 - 20 e^-/nm. This is rather highly charged and is close to the Manning condensation limit. TMV is also optically anisotropic and

exhibits form birefringence as a consequence of its shape anisotropy [22]. TMV has a host of other anisotropic physical properties including diamagnetic and dielectric susceptibilities as well as anisotropic translational diffusion constants, summarized in Table 1.

Electron micrographs of fd reveal a slender thread-like polymer, often bent but without hairpins [23]. The bacteriophage fd is longer and thinner than TMV, with $L = 880$ nm and $D = 6.6$ nm [24] and unlike TMV, light scattering studies show fd is flexible with a persistence length of $P = 2200$ nm [20, 21, 25, 26]. While TMV is composed of multiple copies of only one protein, fd is composed of five proteins. About 2700 copies of one protein comprise the coat, while five copies each of the other proteins make up the ends. The main protein forms a hollow cylinder of outer diameter 6 nm and inner 2 nm, which is filled with the single stranded DNA. fd is also a polyelectrolyte with charge densities similar to TMV [27]. The physical properties of fd are summarized in Table 1. Pf1 has a structure similar to fd and has the same diameter and charge density, but it is longer with a length of $L = 1980$ nm.

The length of the particles can be altered. TMV can be induced to end-to-end aggregate irreversibly by placing it in a dilute lead solution. This results in a polydisperse suspension with particles of lengths of several microns. As far as is known, TMV always aggregates end-to-end producing a polydisperse suspension composed of particles of discrete lengths. TMV can also be fragmented through sonication resulting in a polydisperse suspension of variable lengths, all less than the 300 nm length of native TMV.

The length of fd has been altered using recombinant DNA techniques and there are reports in the literature of mutants strains with lengths up to 3.4μm [28]. This allows us to control the physically important parameter of length, while still maintaining the monodispersity of a biological species.

We have the impression that TMV aggregates much easier than fd and in fact we have very little evidence of any aggregation at all in fd. Perhaps the biological origin of this comes from the fact that TMV is composed of multiple copies of a single protein and thus the ends of the virus are not very different from the middle. Since the viruses self-assemble there is a tendency for TMV to continue to grow. The finite length of the RNA strand terminates growth of TMV, and removing the RNA leads to a polydisperse distribution of protein aggregates. In contrast, fd has several specialized proteins at each end, providing a mechanism to inhibit growth as well as end-to-end aggregation.

Property	Symbol	TMV	fd
diameter	D	180Å [19]	66Å [24]
length	L	3000Å [19]	8800Å [24]
persistence length	P	$> 10L$ [20]	22000Å [26]
density	ρ	1.37 g/cc	
molecular weight	M_w	4×10^7 g/M [29]	1.64×10^7 g/M [30]
Svedburg	S	$188[10^{-13}]$ sec [29]	$47[10^{-13}]$ sec [30]
refractive index increment	dn/dc	0.194 cc/g [29]	
optical density	O.D.	$3.06^{1\,mg/ml}_{1\,cm,265nm}$ [29]	$3.84^{1\,mg/ml}_{1\,cm,269nm}$ [24]
refractive index	n	1.57 [22]	
specific birefringence	$\Delta n/c$	2×10^{-5} cc/mg [8, 31]	6×10^{-5} cc/mg [32]
Diamagnetic anisotropy	$\Delta\chi$	2.0×10^{-9} c.g.s. [9]	7×10^{-24} J/T^2 [32]
charge	e	$2e/Å$ at $> $ pH 7 [33]	$2e/Å$ at $> $ pH 7 [27]
Hamaker constant	A_H	$5 - 9 \times 10^{-14}$ [33]	
permanent dipole moment	μ	2.5×10^{-14} esu cm [34]	
electric polarizability anisotropy	$\alpha_{\parallel} - \alpha_{\perp}$	3.3×10^{-13}cm^3 [31]	
rotational diffusion	D_r	318 ± 3 sec^{-1} [34]	20.9 s^{-1} [30]
average translational diffusion	D_o	4.19×10^{-8}cm^2/sec [35]	2.58×10^{-8}cm^2/sec [30]
parallel diffusion	$D_{\parallel}$	5.38×10^{-8} cm^2/sec [35]	
perpendicular diffusion	$D_{\perp}$	3.59×10^{-8} cm^2/sec [35]	

TABLE 1. Physical constants of TMV and fd

2.1. VIRUS PRODUCTION

Production of monodisperse TMV, fd, and pf1 is not challenging for a biologist. For TMV, we follow the recipe of Boedtkar and Simmons [29], while paying attention to the caveats of Kreibig and Wetter [36]. Basically, we

grow a crop of wild Turkish tobacco plants until they are several weeks old, or about 20 cm in height and then infect the leaves with some TMV (commercial tobacco plants are bred to be resistant to TMV). After another few weeks the plant develop brownish legions indicating infection with TMV. The leaves are ground to extract the tobacco juice and then purification of TMV from the plant debris is achieved by several cycles of differential centrifugation. Low speed spins sediment heavy debris and leave the virus is suspension, and then high speed spins pellet the virus leaving low molecular weight components in suspension. We get about 0.2 g of purified virus from 1 kg of tobacco leaves. The degree of monodispersity of extracted TMV varies from crop to crop. We find that high temperatures ($> 40°$ C) in the green house produces poor samples, and the virus seems most stable at low ionic strength, such as distilled water. Barring catastrophes, or infection with bacteria or mold, TMV samples are stable for years. Extracted samples should never be frozen, as this severely damages the virus. Several times refrigeration malfunctions froze our samples and ruined months of work.

fd and Pf1 are bacteriophages that infect *Escherichia coli* and *Pseudomonas aeruginosa*, respectively. Production of the phage is similar and standard in molecular biology [37]. One produces a healthy batch of bacteria and infects them with virus. After a few hours the bacteria is separated from the virus with a low speed centrifugation spin, and the virus is concentrated with a subsequent centrifugation spin. Yields of about 1 g of virus per liter of infected bacteria are typical. Working with the genetically engineered virus is more difficult; yields are lower and there is a tendency for the bacteria to delete the altered DNA. However, there are ways of applying selective evolutionary pressure to the bacteria to suppress this tendency [28].

Characterizing sample polydispersity is very important in our studies and we have tried a variety of methods including size exclusion column chromatography, light scattering, electron microscopy, magnetic birefringence, analytical centrifugation, and gel electrophoresis. Our current opinion is that electrophoresis [38] offers the greatest resolution in determining the relative size distribution, but must be used in conjunction with electron microscopy to determine the absolute length distribution of the virus.

3. The Isotropic - Nematic transition

The first ordered phase that appears in virus suspensions with increasing concentration is the nematic phase (TMV, pf1) or cholesteric phase (fd). A microscopic theory for the isotropic - nematic (I - N) transition of hard, rigid rods was first developed by Onsager [39] who was actually seeking to

explain the nematic phase in suspensions of TMV. In hard particle suspensions the free energy is determined solely by entropy. Onsager showed that the I - N phase transition results from a competition between two types of entropy; rotational entropy, which is maximized by having the rods point in any given direction with equal probability, and translational entropy, which is maximized by allowing the greatest translational motion, or smallest free volume per rod. In dilute suspensions, the rods move unhindered by their neighbors, irregardless of their relative orientation and the total entropy is maximized with an isotropic angular distribution of rod axes. However, with increasing concentration the randomly oriented rods bump into each other restricting their translational freedom. Eventually, a concentration is reached where the total entropy is maximized by aligning the particles, which reduces the excluded volume per particle and increases the translational entropy at the cost of reducing orientational entropy.

The relevant dimensionless concentration controlling the I - N transition is the excluded volume in the isotropic phase ($b = \pi L^2 D/4$) times the number density (c) and Onsager showed that in the limit of $L/D \gg 1$ the I - N co-existence concentrations were $bc_i = 3.3$ and $bc_n = 4.2$. Note that this transition is temperature independent and the co-existence concentrations depend only on the length and diameter of the particles. A suspension where concentration rather than temperature is the thermodynamic variable is known as a lyotropic.

The virus particles are charged, which has two effects on the I - N transition. First, at a given ionic strength Onsager argued that the free energy of the electrostatic repulsion between particles is equivalent to increasing the diameter of the particle by the distance at which the interparticle repulsive potential falls to kT, this distance being known as the effective diameter D_{eff}. Second, the angular-dependent potential between two like charged cylinders acts to misalign the particles and its magnitude is characterized by the "twist" parameter $h = \kappa^{-1}/D_{eff}$, with κ^{-1} being the Debye screening length [40]. This torque on the particles acts to destabilize the nematic phase and indeed if $h > 4/3$ the nematic phase ceases to exist [41]. To first approximation, Onsager showed that the phase co-existence results for hard rods remain valid for charged rods, but D_{eff} is substituted for D in the excluded volume, b.

The effective diameter and twisting constant h for fd are plotted in Figure 3. At 1 mM ionic strength D_{eff} is about 10 times the hard particle diameter of 6.6 nm, but D_{eff} decreases very rapidly with ionic strength (note the log scale). There is very little variation in D_{eff} with charge density in the range of 5 - 20 e^-/nm because of condensation of the counter-ions. The twist constant h is small, 0.16 at most, and decreases with increasing ionic strength. A similar plot for TMV is given in reference [9] and details of the
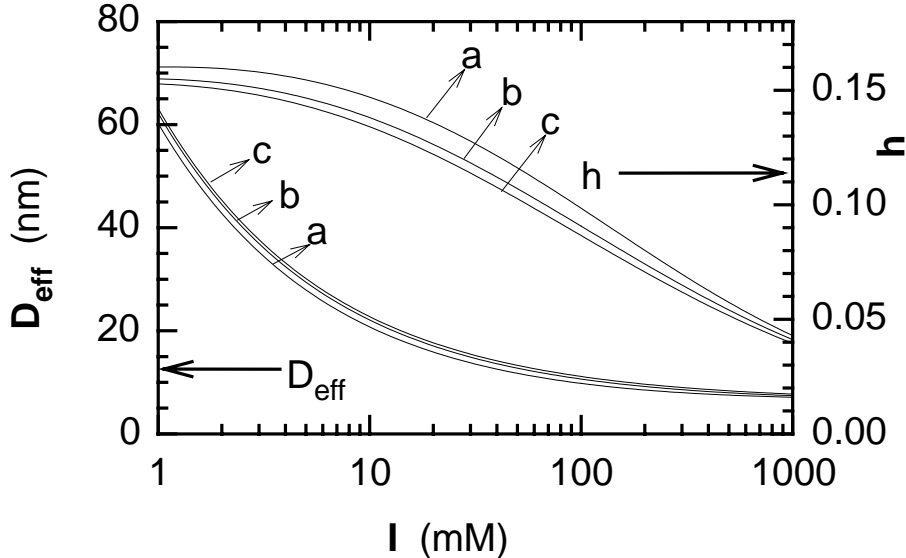
Figure 3. The effective diameter D_{eff} and twisting constant $h = \kappa^{-1}/D_{\mathrm{eff}}$ for fd as a function of ionic strength. The bare diameter of 6.6 nm is approached at high ionic strength. Three charge densities are plotted (a) 5, (b) 10, and (c) 20 $e^-/$nm.

calculation are given in reference [40].

The Onsager theory is restricted to two-body interactions and is thought to be quantitatively accurate only for $L/D_{\mathrm{eff}} > 100$ [1]. We cannot expect the Onsager theory to apply for TMV since $L/D_{\mathrm{eff}} < 17$. However, it is expected that hard rods with $L/D < 100$ also form nematic phases since three-body and greater interactions increase the excluded volume of the isotropic phase, which will act to stabilize the nematic phase [42]. Of course, with decreasing L/D the point will arrive at which the difference in excluded volumes is no longer great enough to stabilize the nematic and a crystalline phase will replace the nematic as the first ordered phase [43].

3.1. CO-EXISTENCE CONCENTRATIONS OF TMV

TMV was the first virus isolated and shortly afterwards it was realized that TMV suspensions formed liquid crystals [44]. This last reference paper has a memorable photograph of the birefringent wake of a gold fish swimming in a TMV suspension. However, the early studies on co-existence concentrations of TMV were done on polydisperse samples, which complicates comparison

with the Onsager theory. A synopsis of previous work on the I - N transition can be found in ref. [9], while ref. [12] focuses on the colloidal crystalline phase. The research described in Section 3 can be found in references [9], [45], [46], and [47].

Having obtained monodisperse samples of TMV, we dialyze the virus against a variety of buffers and adjust the concentration until co-existing phases are found, which are identified by observation through crossed polarizers. If a sample of average concentration slightly greater than c_i is in the initial stages of phase separation, then when viewed with a polarizing microscope the nematic droplets appear as bright footballs of the United States variety on a dark background [12, 44]. With time the nematic domains coalesce and form a continuous phase, which settles to the bottom of the container because the nematic phase is denser than the isotropic phase. To determine the sample concentrations we extract a portion of each phase with a pipette and measure the optical density of the solution to obtain a mass density. We denote the mass densities of the co-existing isotropic and nematic or cholesteric phases as ρ_i and ρ_n, respectively. If the samples are monodisperse then we can convert mass to number density given the molecular weight and density of the virus (Table 1). The I - N phase diagram as a function of ionic strength is shown in Figure 4.

We clearly see in Figure 4 that the measured values are significantly lower than predicted by the Onsager theory. There are several features of the data which agree with the Onsager theory. First, the Onsager theory predicts that ρ_i is inversely proportional to D_{eff} and the trend of increasing concentrations with increasing ionic strength is observed. Second, the width of the co-existence region $w = (\rho_n - \rho_i)/\rho_i$ is similar to the Onsager predicted value of 1.24. Third, the co-existence concentrations were observed to be independent of temperature as long as the virus particles did not begin to aggregate [9].

Since TMV has a small ratio of L/D the co-existence concentrations are expected to be lower than predicted by a theory that neglects higher order excluded volume interactions [42]. There are several theoretical approaches to account for the higher virial terms in hard rod systems of small axial ratio. Instead of using an ideal gas as the reference state, the other choice is to use the liquid of hard spheres as the reference state and include the nematic interaction at the level of the second virial coefficient. We refer the reader to the recent review article of the Onsager model and its extensions by Vroege and Lekkerkerker [1]. In Figure (4) we use a theory developed by Lee [48], which essentially amounts to an interpolation between the accurate limiting theories of the Carnahan-Starling equation of state for hard spheres and the Onsager equation of state for infinitely long hard spherocylinders. This theory accounts in some fashion for the higher virial terms
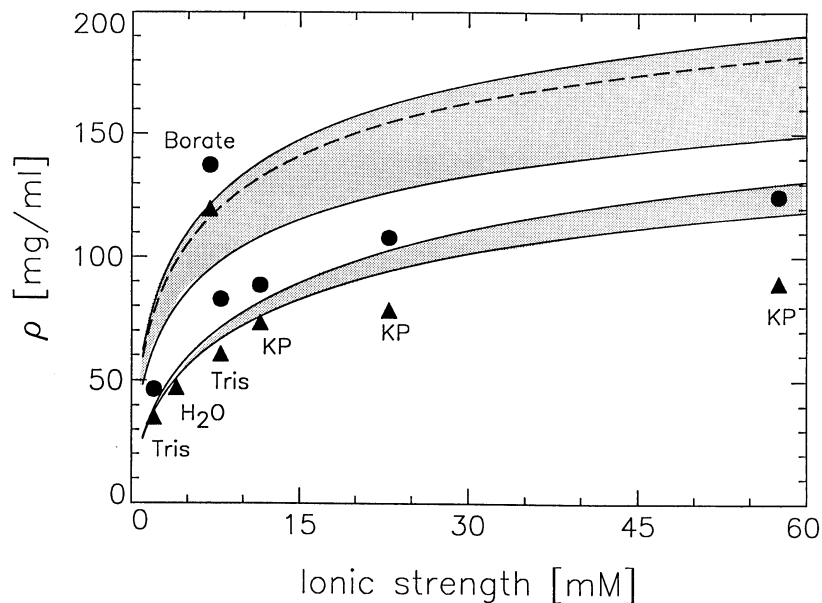
Figure 4. The theoretical isotropic (ρ_i) - nematic (ρ_n) co-existence region for TMV modeled as a sphero-cylinder of dimensions L = 282 nm and D = 18 nm and linear charge density 20 e/nm are plotted for the Onsager theory (upper shaded region) and the theory of Parsons - Lee [9] (lower shaded region). The dashed line (–) is the calculated value of the spinodal branch of the isotropic line and is identical for the two theories. The individual points correspond to measured values of ρ_i ($\triangle$) and ρ_n ($\bullet$). All these samples were experimentally characterized to be monodisperse, including the TMV in borate buffer. The solvent of the TMV suspension is indicated next to the data points. Tris: TRIS - HCl, pH 8.0, KP: Potassium Phosphate, pH 7.2, Borate: Borate buffer, pH 8.5, H_2O: unbuffered distilled water.

in the free energy and lowers the co-existence concentrations, however the predicted width of the co-existence region is much narrower than measured. Experimentally, residual polydispersity or effects of charge may account for this discrepancy; or the theory needs to be improved. We are currently mapping the entire phase diagram of monodisperse TMV, including the I - N transition using monovalent salts, which ease calculations of the effective diameter.

3.2. CO-EXISTENCE CONCENTRATIONS OF FD

There are two notable differences between TMV and fd that need to be discussed before the co-existence data can be analyzed. First, fd forms a cholesteric phase in distinction to the nematic phase for TMV. Second, fd is a flexible particle.

The local arrangement of molecules in the cholesteric phase is similar to the nematic phase except that because the cholesteric is composed of chiral molecules there is on average a small angle of constant sign between the rods. As a consequence, the structure of the cholesteric has a screw axis superimposed normal to the preferred molecular direction [49]. The pitch of a cholesteric is defined as the distance along the screw axis in which the local director has rotated by 360 degrees. For the case of a cholesteric that has a pitch much larger than the intermolecular spacing, the energy of the twist distortion in the cholesteric contributes only a minute perturbation to the total energy associated with the parallel alignment of the molecules [49]. In particular, cholesteric fd suspensions have about 1000 particles per turn of the pitch. One therefore expects that any theory of the isotropic-nematic phase transition will be equally applicable to the isotropic-cholesteric transition.

Flexibility has a more significant effect on the I - N transition. TMV was shown not to satisfy the Onsager model because the length to diameter ratio was too small. However, a particle of any material with $L/D > 100$ will be flexible, and fd with $L/D = 140$ has a persistence length $P = 2.5L$. This is a fairly stiff polymer, but even a modest amount of flexibility can have dramatic effects on the I - N transition. The Onsager theory was extended to account for flexibility by Khokhlov and Semenov (KS) [50, 51] and is valid as long as L and P are much greater than D. In the KS model, the excluded volume term of the Onsager free energy remains the same, except that the contour length of the particle is replaced with the persistence length and the number density with the density of persistent segments. The main modification to the free energy comes from the single particle entropy. For rigid rods, this consists only of rotational entropy, but flexibility adds an additional term. In the isotropic phase the polymer can bend in any direction, and does so on a length scale of a persistence length. However, in the nematic phase the polymer is constrained to bend on average along the nematic director, with the distance between bends known as the deflection length [41]. This constraint lowers the entropy of the nematic phase and thus acts to destabilize its formation. The nematic transition of semi-flexible polymers occurs at higher concentrations than for rigid particles and the co-existence concentrations are narrower.

Khokhlov and Semenov solved their model analytically in the worm-

like limit of $L \gg P \gg D$ and Chen [52] numerically solved the KS model for arbitrary flexibility. The effect of charge on the I - N transition has been calculated in the worm-like limit [53]. To extend the numerical results of Chen for hard polymers to charged polymers, we adopt the Onsager approach, and simply replace D with D_{eff}, as well as neglecting the twisting term h. We expect inclusion of h would shift the co-existence region to slightly greater concentrations [53].

Figure 5 shows the isotropic - cholesteric co-existing concentrations, ρ_i and ρ_c of fd as a function of ionic strength [45]. Theoretical curves are from the numerical results of Chen [52] as described above with D_{eff} taken from Figure 3. The ionic strength stops at 170 mM ionic strength above which serious aggregation was observed through the increase in scattering of the suspension. Although no free parameters are used in the comparison of theory and experiment, we note that D_{eff} is calculated assuming 10 e/nm. However, D_{eff} is insensitive to the value of the charge density for the range of values consistent with titration measurements [27].

In Figure 6, the measured difference of the co-existence concentrations relative to ρ_i, $\omega = (\rho_c - \rho_i)/\rho_i$, is plotted as a function of the ionic strength I. Despite the experimental error, we have repeatedly measured the ratio ω to average approximately 10%. This is at least twice as large as the value from the Khokhlov and Semenov interpolation [50], but falls into close agreement with Chen's numerical result, which is $\omega = 9.9\%$ for $L/2P = 0.2$. The co-existence width ω increases from about 5% to 15% as ionic strength varies from 1 to 170 mM. Two explanations for the increase in ω with ionic strength come to mind. First, as mentioned previously, fd visibly aggregates at ionic strengths greater than 200 mM, and one could expect the onset of aggregation to begin at lower ionic strength. Aggregation can lead to length polydispersity, and as discussed by Lekkerkerker in these lectures, the co-existence width ω can increase dramatically with the addition of small amounts of long aggregates [1, 54]. A second explanation is that the increase of ω with ionic strength is a consequence of the twisting effect of the electric interaction between the charged rods. We observe that the smallest values of ω occur at the lowest ionic strength where the twisting constant h is the largest. This would be expected since large values of h act to destabilize the nematic phase [40, 41].

3.3. TEMPERATURE DEPENDENCE OF THE CO-EXISTENCE CONCENTRATIONS OF FD

In contrast to TMV, where the isotropic - nematic co-existence concentrations were temperature independent [9], we observed that for fd the isotropic - cholesteric co-existence concentrations varied in a non-monotonic fashion with temperature over the range 4 - 65° C [55, 47]. We studied a
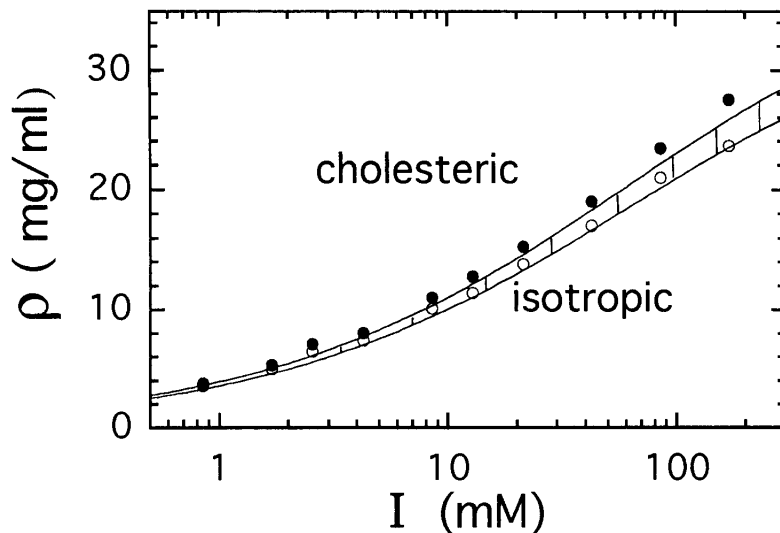
Figure 5. Concentrations of co-existing isotropic (○) and cholesteric (●) samples of fd virus suspensions as a function of ionic strength (I). Theory curves (solid lines) are calculated based on numerical results from Chen [52] using the ratio of contour to persistence length $L/P = 0.4$. The effective diameter is taken from Figure 3 with charge density $10e^-/nm$. Vertical bars indicate the co-existence region.

fd virus solution of approximately 20 mg/ml that was dialyzed against 10 mM potassium phosphate buffer solution at pH 7.3. Phosphate was chosen because of the weak temperature dependence of the pH. However, a disadvantage of phosphate is that it is polyvalent, which complicates the calculation of the interparticle potential [40]. The sample after dialysis was carefully diluted to the co-existence region and sealed with rubber cover in a small clean glass tube of roughly 40 mm in length and 5 mm in diameter. Then the tube was immersed, but kept vertical, in a temperature controlled water tank and allowed sufficient time to phase-separate. The phase separation in the bulk was slow due to the small difference in the specific gravity between the two co-existing phases, and also the viscosity was large due to the length of the virus particles. Frequently, a table centrifuge was used to apply up to 1000 g to speed the separation after the isotropic and cholesteric phases separated into micron sized droplets after standing at 1 g overnight. The temperature at which the sample was equilibrated was not always maintained during centrifugation, so the samples were spun in suc-
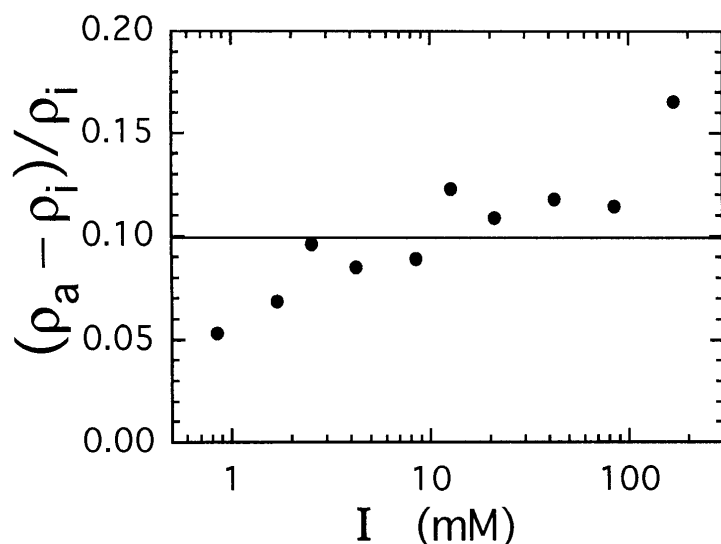
Figure 6. The ratio $\omega = (\rho_c - \rho_i)/\rho_i$ (•) at different ionic strengths. The numerical result, ignoring the twisting effect ($h = 0$), predicts $\omega = 0.099$ (solid line).

cessive intervals of a few minutes each and the sample tube was replaced in the temperature bath immediately following each centrifugation. The time needed for the samples to equilibrate were much greater than the time that the sample was in the non-temperature controlled centrifuge. After thorough phase separation into an isotropic phase in the upper portion of the tube and a cholesteric in the bottom portion, a sample of volume 20 μl or so was carefully taken by pipette from each phase while observing through crossed polarizers. The samples were immediately weighed with an analytical balance of 0.01 mg accuracy and subsequently diluted approximately 50 fold to measure the fd mass concentration by optical spectrophotometry. It was necessary to thoroughly mix the two-phase samples after changing the temperature because it would take an extremely long time for the individual co-existing isotropic and cholesteric phases to change concentration purely by diffusion. In other words, it is easy to superheat or cool these samples, but mixing the samples allows them to reach equilibrium. Repeated measurements showed that the variation of the co- existence concentrations between different samples prepared under what was intended to be identical conditions occasionally reached 5 percent.

In Fig. (7), the I - C co-existence concentrations of fd are shown at five temperatures. A 5% error bar was assigned to each data point, for
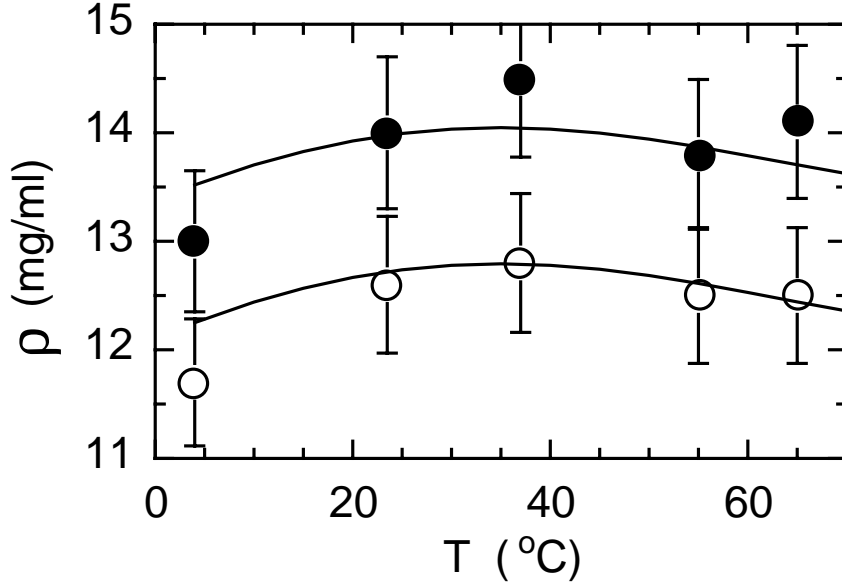
Figure 7. Co-existence concentrations of isotropic ρ_i (○) and cholesteric ρ_c (●), measured at five temperatures. A maximum in co-existence concentrations is observed near $35°$ C. Error bars indicate 5% variation for each concentration.

which three independent measurements were done. However, since we always measured ρ_i and ρ_c in the same sample, the relative difference between the co-existence concentrations, $\omega = (\rho_c - \rho_i)/\rho_i$, was reliably measured to be about $\omega \sim 10\%$ at each temperature. The remarkable feature of the temperature dependence of the co-existence concentrations is that a maximum was observed at about $35°$ C. The temperature induced shift in co-existence concentrations is not large, amounting to about a 5% variation between the highest and lowest concentrations.

An alternative method for determining co-existence concentrations as functions of temperature is to measure the percentage of the cholesteric portion of the sample in co-existence, instead of directly measuring the concentrations as before. Since the capillaries are about 8 cm in length and have uniform cross section, the percentage of cholesteric is easily determined by measuring the ratio of height of the cholesteric to the total sample with a ruler. More importantly, since the fractional difference in concentration between the co-existence phases ω is small, and always about 10%, the shift of percentage of the cholesteric phase is approximately 10 times the percentage change of the concentration of either phase. This magnifying

effect arises from the conservation of the total virus in a sealed capillary, which can be written as

$$\rho_i\,(1-f) + \rho_c\,f = \rho_i(1 + f\,\omega) = \rho_{\text{ave}} \tag{1}$$

with f the fraction of the cholesteric, ρ_i the concentration of the isotropic, and ρ_{ave} the average concentration of the total solution. For example, if following a temperature change the isotropic concentration changes as $\rho_i \rightarrow 0.95\rho_i$, and the width of the co-existence region ω remains 0.1, then f increases by about 50% according to eq. (1). Thus a 5 percent change in the co-existence concentrations is translated into a 50% shift in the height of the co-existence phase boundary.

There is a serious draw back to this method due to the observation of a slight irreversible change of the fd samples with time. At room temperature, the co-existence concentrations shift higher with time, and such a shift persisted for months during our experiment with the sample sealed in capillaries. A day or two is usually necessary to reach complete separation of the new equilibrium phases following every temperature change, in spite of the help of gentle centrifugation. A typical cycle consisting of one measurement following every 5°C temperature change through the temperature range $4 - 70$°C takes 3 to 4 weeks, during which period the co-existence concentrations shift upwards about 1 percent. This is a very slight change, but is easily measured as a change in the height of the I - C meniscus. The rate of shift is dependent on temperature and is larger at high temperatures. At 4°C, the sample stays stable for months. This shift rate also depends on the ionic strength, and we observed more rapid changes at the lower ionic strengths. The physical origin of such a shift is not well understood. We believe, however, it is related to an intrinsic change of fd particles.

Figure (8) shows the percentage of cholesteric phase in one sample capillary as a function of temperature. The temperature was cycled from low to high temperature once (circles), and then from high to low once (triangles). Since the total material in each tube is constant, an increase in the co-existence concentrations results in a decrease of the percentage of the cholesteric phase. From the beginning to the end of the experiment of Fig. (8), a period of two months, the percentage of the cholesteric phase decreases from 70% to 55%, which amounts to only a 1.5% shift in the co-existence concentrations.

We have observed that the co-existence concentrations always increase with time, and with a low but constant rate at each temperature. This suggests a method to compensate for this time dependence without having to know the actual rate of shift at each temperature. One can make two series of measurements, first one consisting of sequential temperature increases and the second of temperature decreases taken in opposite order of
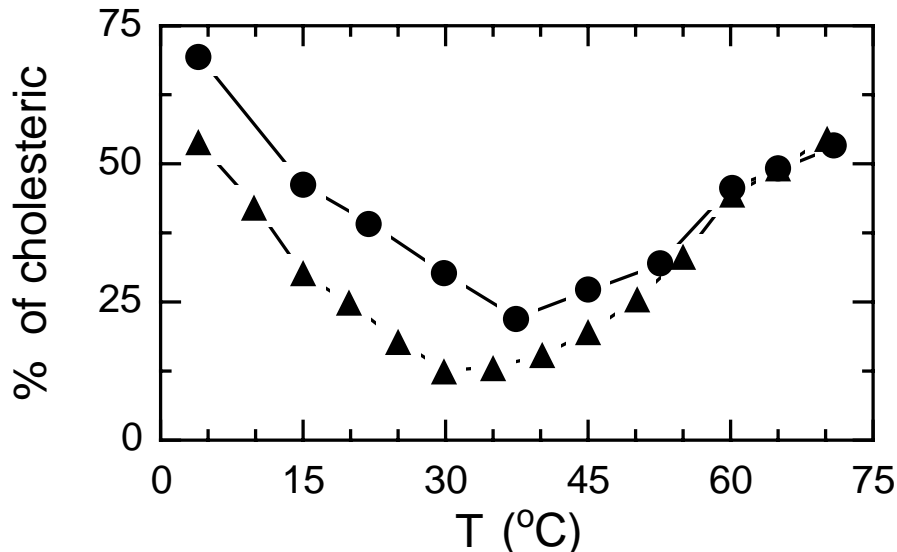
Figure 8. Percentage of the cholesteric in co-existence with the isotropic phase as a function of temperature, measured in a sealed capillary of the total liquid length 82.2 mm. The temperature was cycled once from low to high temperature (circles), and then back from high to low once (triangles). The total experiment was completed in about two months, over which time the percentage of the cholesteric at 4°C decreased about 15%. The decrease in the percentage of the cholesteric phase from $4 - 35°$ C corresponds to an increase in the co-existence concentrations of about 5%, a result consistent with the data of Fig. (7).

the increases and with equal amount of time spent at the same temperature levels. Then, by taking the average of every two measurements at the same temperature, the accumulated drift at all temperatures before and after the measurements at the highest temperature point is exactly canceled. In effect, this method sets the highest temperature concentration as the reference concentration, which is incorrect by only about one percent.

In the previous section we showed how the co-existence concentrations of fd as a function of ionic strength were in excellent agreement with Chen's [52] numerical results of the Khokhlov and Semenov theory [50, 51]. If we accept this theory as being applicable to the fd system, then we conclude that the temperature dependence of the I - C transition arises from the temperature dependence of the flexibility of fd. Chen [52] provides explicit formulae for the dependence of concentration of the co-existing isotropic phase ρ_i and the width of the co-existence concentrations ω as functions of only the ratio of contour to persistence length of the particle. We substitute
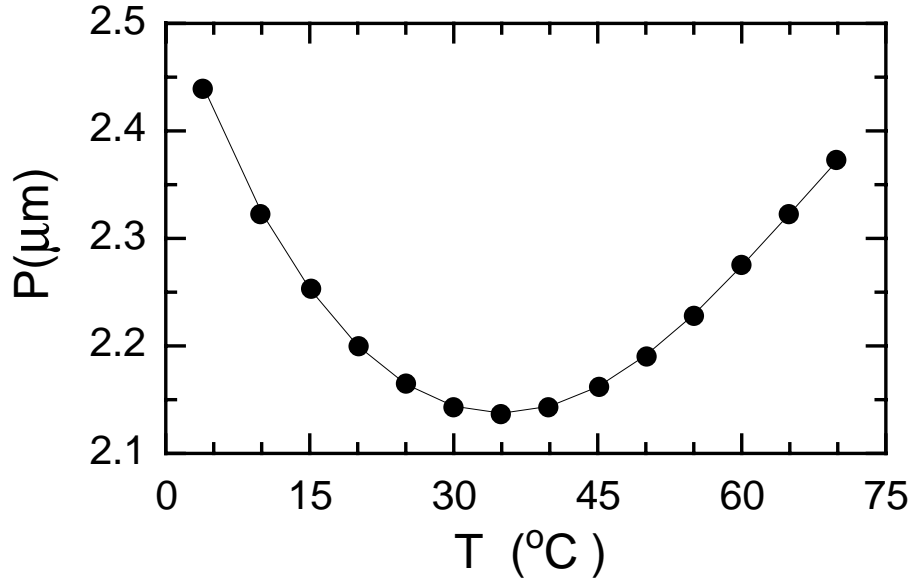
Figure 9. The persistence length P of fd as a function of temperature deduced from the measurements of the percentage of the cholesteric phase in co-existence with the isotropic shown in Fig. (8).

these expressions in eq. (1) along with the measured value of the percentage of the cholesteric phase p to convert eq. (1) into a function whose only unknown is the persistence length P and the temperature independent constant ρ_{ave}. We know $P = 2.2\mu$m at 20° C from the literature, and this fixes the constant ρ_{ave}. We thus convert eq. (1) into an equation that relates the persistence length as a function of the percentage of the cholesteric in a co-existing sample. The values of the persistence length deduced in this fashion are shown in Fig. (9). We find that the persistence length decreases about 15% over the temperature range 4 - 35° C and then increases again by nearly the same amount from 35 - 70° C. It would be interesting if independent confirmation of this result could be made by another technique, such as light scattering.

4. Pre-transitional angular correlations in the isotropic phase

TMV has a positive anisotropy of the diamagnetic susceptibility $\Delta\chi$, which means that the rods tend to align parallel to an applied magnetic field. The particles are also optically anisotropic and when partially aligned by the field the entire suspension becomes birefringent. In the absence of a field,

the particles in the isotropic phase point in all directions with equal probability when averaged over the entire sample and the suspension is optically isotropic. However, locally there are angular correlations between neighboring rods. Application of a magnetic field aligns these correlated regions along the field. How does the field induced birefringence (Δn) depend on the number of particles in a correlation volume? This can be answered by considering Δn from a single rod in a field. Research described in this section can be found in references [9], [45], [47], and [56].

The birefringence for non-interacting rods in a weak field is [57]

$$\Delta n = \frac{c\Delta N'\Delta\chi H^2}{15kT} \tag{2}$$

with c the number density, and $\Delta N'$ the maximum specific birefringence. The total birefringence of a completely aligned solution is $\Delta n_{\text{sat}} = c\Delta N'$, which is proportional to the number density. To determine the effect of correlations on Δn, first consider a solution of identical particles, which have a field induced birefringence given by eq. (2). Now imagine that each particle is highly correlated or bound parallel to just one other particle. Then both $\Delta N'$ and $\Delta\chi$ will double, but c will halve. Thus from eq. (2) Δn will double demonstrating that the field induced birefringence is proportional to the number of particles in a correlation volume.

It is instructive to consider $\Delta n/c$ as the response per particle to an external stimulus H^2. The ratio of this response to stimulus is then the susceptibility of the suspension to align parallel to the field. We define the specific magnetic susceptibility or specific Cotton - Mouton constant to be

$$\text{CM} \equiv \frac{\Delta n}{cH^2} \tag{3}$$

The field induced birefringence of the isotropic phase of a lyotropic liquid crystal was first discussed by Straley [58] in a thorough review article of the experiments and theory of colloidal liquid crystals as of 1973. Straley showed that the specific magnetic susceptibility of hard rods in the limit of zero field for the Onsager approximation is

$$\text{CM} = \frac{\Delta N'\Delta\chi}{15kT(1 - c/c^*)} \tag{4}$$

with $c^* = 4/b$, where $b = \pi L^2 D/4$, the average excluded volume of a pair of rods in the isotropic phase. Analogous to the case of thermotropic liquid crystals, the birefringence would diverge if the concentration c increases to c^*. But before this occurs, the suspension becomes nematic via a first-order phase transition, which in the Onsager model occurs at $c_i = 3.3/b$.

In this model, the specific field induced birefringence is 5.7-fold greater at the I - N transition than when the concentration is zero. This increase in the susceptibility can be interpreted as having the number of particles in a correlation volume (N_{corr}) increase. It follows that N_{corr} is given by the ratio of the susceptibility at finite concentration to the susceptibility in the limit of zero concentration or

$$N_{\text{corr}} = \frac{\text{CM}}{\text{CM}|_{c\to 0}} = \frac{1}{1 - c/c^*} \tag{5}$$

Equation (4) for CM can be generalized to take into account both charge and flexibility [45]. We find an expression similar to equation (5) but with

$$\text{CM}|_{c\to 0} = \frac{\Delta N'\Delta\chi}{15kT}\frac{1}{g(N)} \tag{6}$$

and

$$c^* = \frac{16}{\pi D_{\text{eff}}L^2}\frac{g(N)}{(1 - 3h/4)} \tag{7}$$

with h the twist constant discussed previously and

$$g(N) = \left\{\frac{2}{3N}[1 - \frac{1}{3N}(1 - e^{-3N})]\right\}^{-1} \tag{8}$$

where $N = L/P$ is the number of persistent elements per polymer.

Two simple limits for CM as a function of flexibility are given. For a rigid charged rod, $N = 0$, and

$$\frac{\Delta n}{cH^2} = \frac{\Delta N'\Delta\chi}{15kT}\left(1 - \frac{c(1 - 3h/4)}{c^*}\right)^{-1} \tag{9}$$

with $c^* = 16/\pi D_{\text{eff}}L^2$. In the worm-like limit as $N \gg 1$, $g(N) \sim 3N/2$ asymptotically, and we arrive at equation (9) again with the substitutions $\Delta\chi \to \Delta\chi_P$ and $c \to c_P$, where $\Delta\chi_P = 2\Delta\chi/(3N)$ and $c_P = 2c/(3N)$ are the magnetic anisotropy of a persistent segment and the concentration of persistent segments, respectively.

4.1. MEASUREMENT OF ANGULAR CORRELATIONS

Magnetic birefringence experiments discussed here were done at the Hochfeld Magnetlabor of the Max Planck Institut (HM-MPI) in Grenoble, France and the Francis Bitter National Magnet Laboratory (FBNML), at the Massachusetts Institute of Technology in the USA. At HM-MPI we used a Bitter magnet with a maximum field of 13.5 Tesla and a 3 cm sample path length.

The magnet had a radial access for the laser perpendicular to the field, which simplified the optics and maximized space for the sample. Improvement of the field to 20 T is underway. The detection optics incorporated a photoelastic modulator (PEM) from Hinds International and a Pockels cell with birefringent axes oriented parallel to the field and a crossed polarizer/analyzer pair oriented at $\pm 45°$ with respect to the field. In the absence of any field induced birefringence (Δn) the PEM modulates the birefringence at 50 kHz, which produces an 100 kHz intensity variation since $I \propto \sin^2 \Delta\phi$. The combination of a static field induced birefringence and the PEM produces a 50 kHz intensity variation. The light intensity is detected by a photodiode and the 50 kHz component is isolated by a lock-in amplifier and fed through an operational amplifier to drive a Pockels cell to compensate the field-induced birefringence. The HM-MPI set-up has a very convenient design to facilitate rapid changing of samples, a welcomed feature when studying lyotropic samples.

At FBNML the maximum field is 20 T, but there is no radial access. This limits the path length to 3 mm. For samples for which Δn is linear in H^2, a 3 cm path length - 13.5T magnet produces about 5 times the signal of a 3 mm path length - 20 T one. However, sometimes new physics occurs at high fields - an example of which will be given shortly.

The optics at FBNML consists of two polarizers crossed at $\pm 45°$ with respect to the magnetic field, as well as a 50 kHz PEM and Babinet compensator aligned with optic axes parallel to the field. This is identical to the HM-MPI set-up. The detection scheme at FBNML uses a two lock-in technique, similar to methods that have been discussed by Fuller [59, 60]. This technique allows the birefringence to be measured without using any compensation. The intensity of transmitted light is $I = I_0[1 - \cos(\delta_m + \Delta\Phi)]/2$ with $\delta_m = A\sin(\omega t)$ the time varying retardance induced by the PEM and $\Delta\Phi$ the field induced retardance. If the PEM is the only birefringent object between the polarizers, then the intensity of the transmitted light will vary with frequencies of integer multiples of 2ω. However, once the field induces some additional static birefringence the intensity will have a frequency component at ω. The amplitude of the ω and 2ω components can be calculated with the three following equations:

$$\cos(\delta_m + \Delta\Phi) = \cos(\delta_m)\cos(\Delta\Phi) - \sin(\delta_m)\sin(\Delta\Phi) \tag{10}$$

$$\cos(A\sin(\omega t)) = J_0(A) + 2\sum_{k}^{\infty} J_{2k}(A)\cos(2k\omega t) \tag{11}$$

$$\sin(A\sin(\omega t)) = 2\sum_{k}^{\infty} J_{2k+1}(A)\sin((2k+1)\omega t) \tag{12}$$

Two lock-in amplifiers simultaneously measure the 50 and 100 kHz signals and reject all the other harmonics. Finally, the field induced phase shift $\Delta\Phi$ is found

$$\tan(\Delta\Phi) = C\frac{V_{50}}{V_{100}} \tag{13}$$

with V_{50} and V_{100} the voltage output of the 50 and 100 kHz lock-ins respectively. The constant C is experimentally determined by measuring V_{50} and V_{100} in the absence of magnetic field where $\Delta\Phi$ is produced by a Babinet compensator of a variable, but known retardance. This technique is extremely sensitive, the constant C is independent of the incident intensity I_0, and several orders of retardation are easily accommodated.

An ideal magnetic birefringence set-up designed for lyotropic samples would have a $\sim$ 50 mm bore magnet with radial access for the light, and 20 T maximum magnetic field. This would permit a 3 cm sample path length, while preserving enough room to provide temperature control of the sample. The double lock-in detection method seems to work a bit better than the compensation method, and permits measurements of retardance greater than 2π.

4.2. PREVIOUS PRE-TRANSITIONAL MEASUREMENTS

The first study of pre-transitional angular correlations in lyotropics using magnetic field induced birefringence was performed by Nakamura and Okano [61] in fd suspensions. They studied both the magnetic susceptibility and the rotational diffusion of the rods in the isotropic phase over a wide concentration range for one ionic strength and constant temperature. The temperature and concentration dependence of the induced birefringence of TMV for dilute samples was first carried out by Photinos et. al. [62]. In our work we have extended these previous measurements to measure the field induced birefringence as a function of concentration, ionic strength, and temperature over the entire isotropic phase for both TMV and fd [9, 45].

4.3. TEMPERATURE DEPENDENCE OF THE MAGNETIC BIREFRINGENCE.

In all the preceding, we have assumed that the degree of alignment by the magnetic field is small, which means that the field induced birefringence should be proportional to H^2. In Figure (10), the induced birefringence versus the square of the field is plotted for two concentrations of virus, and two temperatures. The proportionality between the square of the field and the birefringence is clearly shown, as predicted by eq. (9). One can further note that the slope of these curves ($\Delta n/H^2$) increases as concentration increases or temperature decreases.
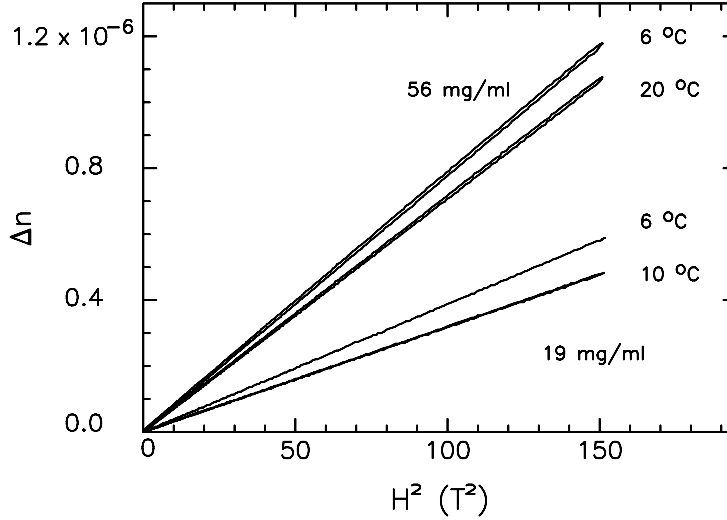
Figure 10. Magnetic field induced birefringence (Δn) of TMV is proportional to the square of the field (H^2). The samples are in 25 mM phosphate buffer at pH 7.2 and concentrations of 56 and 19 mg/ml and at the temperatures indicated. The traces are digitized recordings of sweeping the field up to and down from 12.3 tesla in one minute.

The susceptibility to alignment per particle is found by determining the slope $\Delta n/\rho H^2 \equiv$ CM from data such as shown in Figure (10). To experimentally determine the mass concentrations ρ we measure the optical density in the ultra-violet, which is sensitive to the total amount of DNA or RNA in the suspension. This can be converted to number density using the known molecular weight of the virus *and* knowing the particle size distribution. Only if the samples are monodisperse is there a simple relationship between number and mass density; $\rho = cm$, with ρ the mass density of virus, c the number density, and m the molecular weight of the virus. In Figure (11) the inverse specific Cotton-Mouton constant 1 / CM is plotted as a function of temperature for a range of concentrations of TMV from dilute to co-existence with the nematic. According to eq. (4) there should be a family of straight lines whose slope decreases with increasing concentration and with 1/CM = 0 at $T = 0°$ K. We do see straight lines with decreasing slope, but 1/CM = 0 at $T^* = 115°$ K. We argue that this is due to a temperature dependence of $\Delta\chi$, and not to any collective behavior [9] because we observe that T^* does not vary with either concentration or ionic
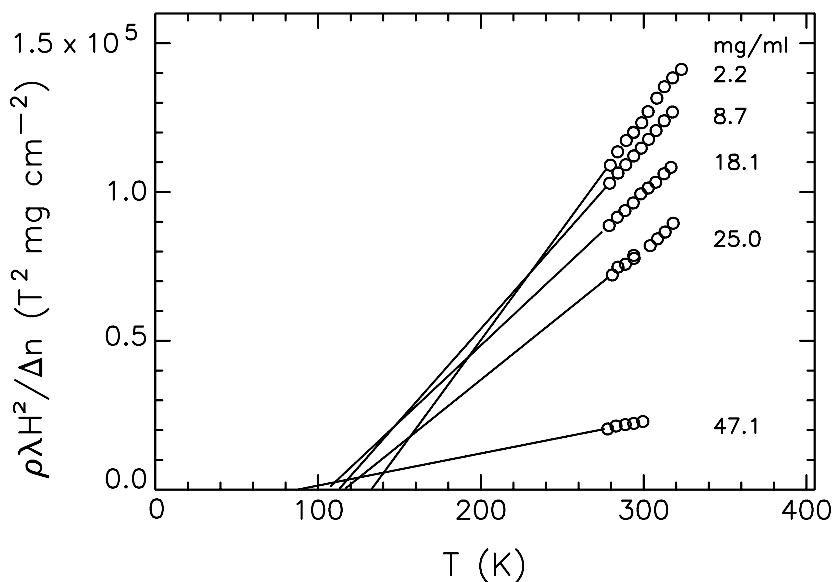
Figure 11. The inverse specific magnetic susceptibility (λ/CM) is shown as a function of absolute temperature (T) for isotropic suspensions of TMV in unbuffered water. The wavelength of light $\lambda = 633$ nm is placed in the numerator by convention. The highest concentration, 47 mg/ml, is in co-existence with the nematic phase. The values of λ/CM were reversible within the temperature ranges shown for each concentration and fall on a line which extrapolates to zero at $T^* = 115 \pm 20\,^{\circ}K$.

strength. Furthermore, we believe that the temperature dependence of the CM constant involves internal rearrangement of the orientation of the nucleic acid bases, which does not alter the flexibility or persistence length of the whole particle, because the I - N co-existence concentrations were observed to be temperature independent.

At low values of the field a proportionality between Δn and H^2 is also observed for fd suspensions. In Figure (12) the specific susceptibility times temperature is plotted as a function of temperature for several concentrations. According to eq. (4) this combination should be temperature dependent. Instead we observe that there is a non-monotonic variation with a minimum at about 35° C. Similarly to the TMV case, we argue that this arises from a temperature dependence of the CM constant of fd, and not to any collective pre-transitional behavior [55, 47] because the data from dilute samples in Fig. (12) also show a minimum demonstrating that the non-monotonic behavior of the CM constant is a single particle property. The magnitude of the temperature variation of the CM constant is con-
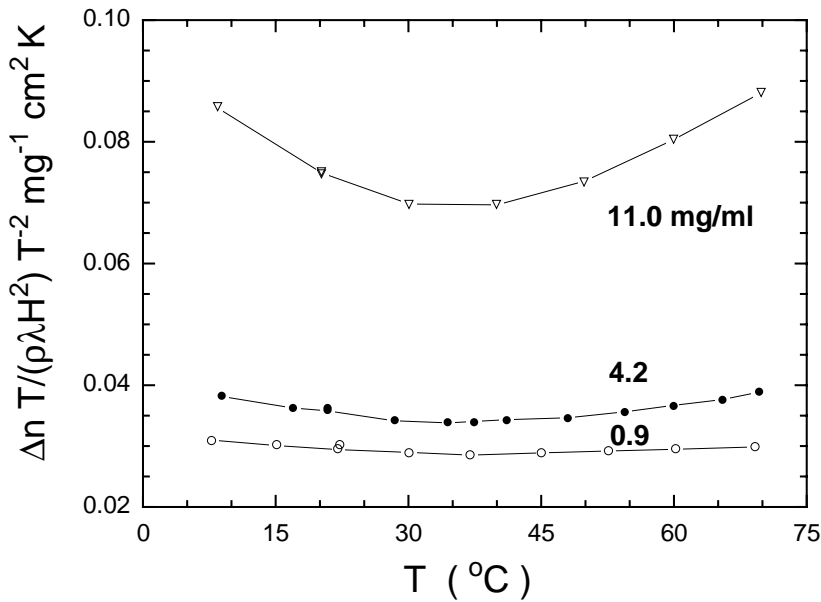
Figure 12. $\Delta n\,T/(\rho\lambda H^2)$, the product of the specific Cotton-Mouton constant (eq. 3) and the absolute temperature divided by the wavelength of light λ, as a function of temperature for fd suspensions. Eqs. (4-8) predict that temperature dependence in this plot can arise from either a temperature dependent $\Delta\chi$ or persistence length of the particles. Curves with three concentrations are shown in the graph. Each curve shows a well defined minimum at about 35^0C. We interpret this to mean that the flexibility of fd has a maximum at this temperature.

sistent with and independently confirms our previous interpretation that the temperature dependence of the co-existence concentrations of fd arises solely from changes in the flexibility of individual particles. The observed concentration dependence of the CM constant, discussed next, is as predicted due to pre-transitional angular correlations.

Both TMV and fd showed variations of $\Delta\chi$ with temperature. In general, the origin of this variation is the rearrangement of the molecules responsible for the value of $\Delta\chi$. Variation of $\Delta\chi$ with temperature can arise from a temperature dependent flexibility or persistence length, or can arise from reorientation of only a small subset of molecules internal to the particle, which are responsible for the $\Delta\chi$. In the latter case, a temperature variation of $\Delta\chi$ does not necessarily mean that the flexibility of the particle is varying with temperature. For the case of TMV, the RNA comprises only a few percent of the total mass of the particle but is entirely responsible for $\Delta\chi$, since upon removal of the RNA from the protein coat the sign of $\Delta\chi$ changes from positive to negative. A combination of observations of

the isotropic - nematic (cholesteric) phase transition with temperature and the temperature variation of the field induced birefringence has lead us to the following two conclusions. We find that for TMV the temperature dependence of the CM constant arises solely from internal rearrangement of molecules, and the flexibility of TMV is independent of temperature. For fd, in contrast to TMV, we find that the temperature dependence of the CM constant arises solely from the temperature variation of the persistence length of fd, and not from internal rearrangement of molecules.

The important conclusion of these temperature studies is that while temperature does effect single particle properties, such as the $\Delta\chi$ of TMV and the persistence length of fd, temperature does not otherwise influence pre-transitional correlations and the phase transition.

4.4. CONCENTRATION DEPENDENCE OF THE PRE-TRANSITIONAL CORRELATIONS

Having determined that temperature does not influence the pre-transitional correlations, it follows that to study the correlations through measurements of the magnetic susceptibility as a function of concentration and ionic strength, it is only necessary to measure the Cotton - Mouton constant at one temperature for each concentration. In this study, all measurements were carried out at 20°C. In Figure (13), the measured 1/CM values (individual points) as a function of TMV concentration for four different ionic strengths are shown. The lowest ionic strength was achieved by placing ion-exchange resin in contact with the TMV solution, in which case the only ions present are the hydrogen counter-ions of TMV. The concentrations of all samples, but the one in ion-exchange resin, span the entire isotropic range.

There are several features to note about the data of Fig. (13). First, the value of 1/CM at $\rho = 0$ is slightly different for the four samples, indicating a small degree, although non-negligible, amount of polydispersity. Second, the concentration dependence of 1/CM is a strong function of ionic strength. The excluded volume, $b = \pi L^2 D_{\mathrm{eff}}/4$, which is proportional to the initial slope of the curves in Figure (13), increases over sixteen times from the case of the suspension in 25 mM phosphate buffer (57.5 mM), to the suspension kept in de- ionized water (resin) where the ionic strength is provided only by the counter-ions of TMV. Third, the three data sets which span the entire isotropic phase decrease faster than a linear function of concentration. If the rods had a large enough axial ratio (L/D) such that only two body interactions were important, then 1/CM would be described by eq. (4) and would be linear in the TMV concentration. The observation of a non-linear concentration dependence of 1/CM implies that terms greater than the second virial coefficient are important in the I-N phase transition for

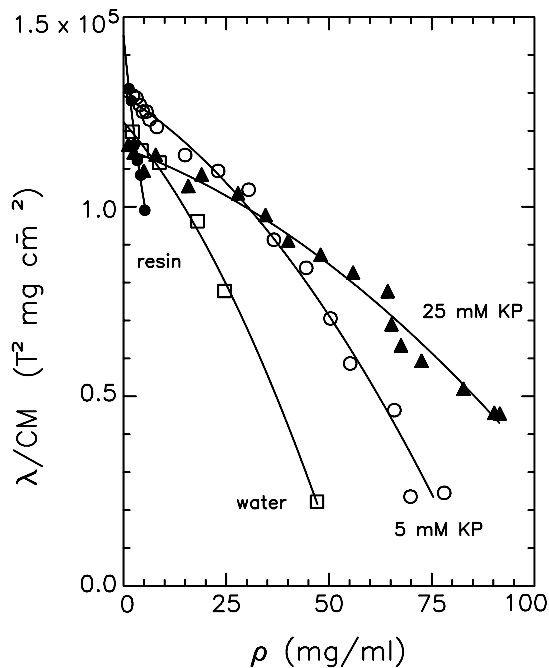*Figure 13.* The inverse specific magnetic susceptibility (λ/CM) as a function of concentration (ρ) at constant temperature ($T = 20\,^\circ$C) was measured for four ionic strengths for monodisperse samples of TMV. The symbols correspond to: ($\bullet$) TMV in ion exchange resin, (square) unbuffered water, (o) 5 mM potassium phosphate buffer, pH 7.2 (KP), and ($\triangle$) 25 mM KP. The solid lines are fits to the Parsons - Lee theory. The last three samples cover the entire isotropic range.

TMV, which indeed was expected for rods with $L/D < 100$. Fourth, the highest concentration shown (except for the resin sample) is for the isotropic phase in co-existence with the nematic phase. The expected trend, that the transition concentrations increase as ionic strength increases, is observed. Fifth, N_{corr} (eq. 5) or the number of particles in a correlation volume varies between 3 and 6 (see Figure (15)).

In Figure (14), the measured 1/CM values (individual points) as a function of fd concentration for five different ionic strengths are shown. In contrast to Figure (13) for TMV, 1/CM is a linear function of ρ, as predicted by the Onsager theory and eq. (4). This is because fd has a value of L/D ten times that of TMV. The limit of concentration of stability of the isotropic phase, ρ^* is found by fitting the 1/CM data to eq. (4) and extrapolating to the concentration where 1/CM = 0.

In Figure (15) the number of particles in a correlation volume is plotted as a function of concentration for TMV where the data is derived from
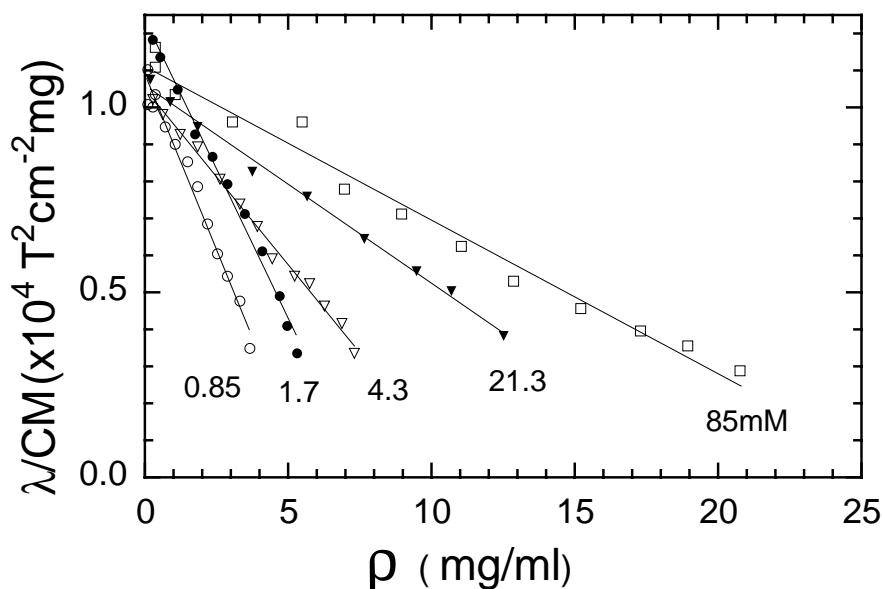
Figure 14. The inverse of the specific Cotton-Mouton constant (λ/CM) versus fd concentration ρ. The five curves correspond to the five ionic strengths labeled on the plot in units of milli-molar (mM) with the buffer being Tris-Cl at pH 7.5. In all cases the highest concentration is at the isotropic-cholesteric phase transition. Each group of data is fit to eq. (4) and extrapolated to obtain ρ^*, the concentration where 1/CM = 0.

Figure (13) using eq. (5). There have been several detailed computer simulations on fluids of ellipsoids and spherocylinders with $L/D = 5$ for which N_{corr} was calculated [63, 64] at the I-N transition. The value of N_{corr} was difficult to determine due to the slowing down of the dynamics near the phase transition. One measurement on a system consisting of 576 particles after 20,000 trial moves per particle gave $N_{\text{corr}} = 5.8$ [63] while a longer run of 50,000 moves per particle yielded 2.6 [65]. In Figure (15) the data of Frenkel for N_{corr} versus mass concentration (ρ) for spherocylinders with $L/D = 5$ is plotted along with the values predicted by the theory of Lee for hard particles of the same aspect ratio. There are no free parameters when comparing the theory with the computer simulations.

In Figure (16) the number of particles in a correlation volume is plotted as a function of concentration for fd where the data is derived from Figure (14) using eq. (5). The solid lines are not fits of the data, but predictions of the theory with zero adjustable parameters.

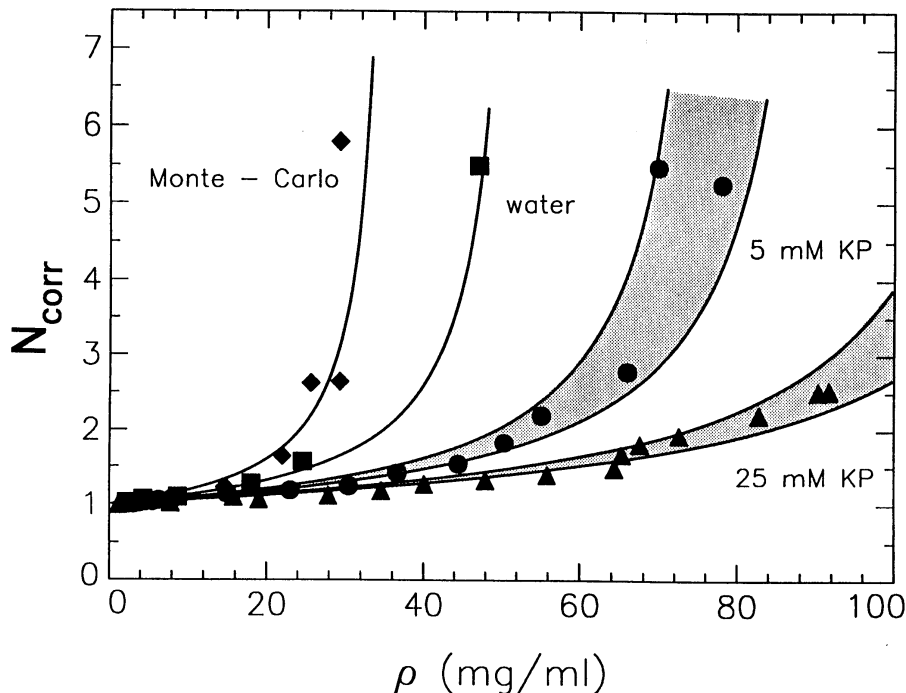Finally, in Figure (17) the phase diagram for fd is shown again with

Figure 15. The number of TMV particles in a correlation volume N_{corr}, experimentally obtained using eq. (5) is shown as a function of weight concentration, ρ. The solid lines are the theoretical predictions of the Parsons - Lee theory. The symbols represent: (diamonds) Monte-Carlo data for hard spherocylinders of $L/D = 5$, and the other samples are the same as in Figure (13): (square) unbuffered water, ($\bullet$) 5 mM potassium phosphate buffer, pH 7.2 (KP), and ($\triangle$) 25 mM KP. The theory for the Monte - Carlo data has no adjustable parameters. The theory curves for the two phosphate buffer samples were calculated assuming either 5 or 20 e/nm charge density for TMV and using the known ionic strength of the buffer.

the additional points of the spinodal of the isotropic phase ρ^* obtained from the birefringence data shown in Figure (16). Note that the spinodal concentration for the isotropic phase ρ^* is greater than the co-existence concentration of the nematic phase.

5. Pre-transitional spatial correlations

The Onsager theory ignores spatial correlations between particles and both the isotropic and nematic phases are assumed to be liquid-like with short range correlations. Using low angle neutron scattering we measured the in-
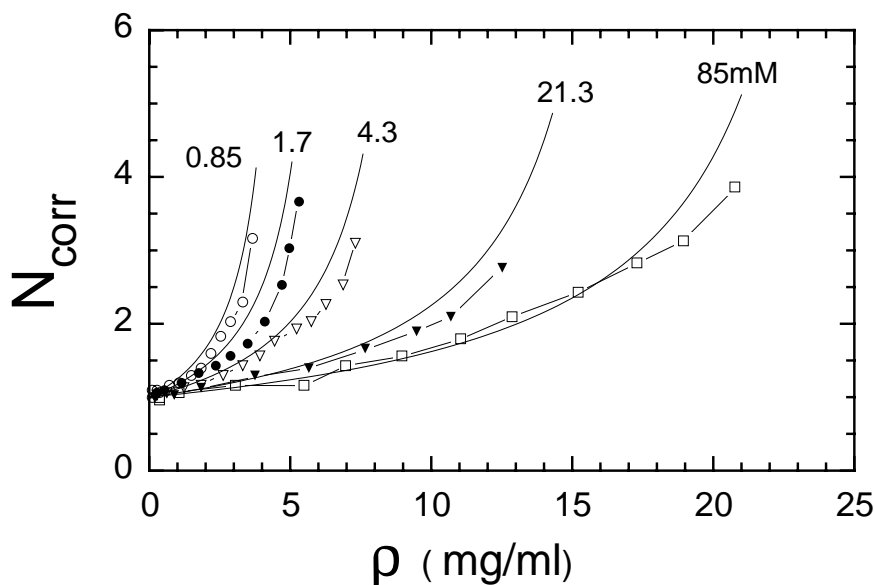
Figure 16. The fd concentration dependence of N_{corr} (eq. 5). Experimentally, N_{corr} varies between 2.5 and 4 at the isotropic - cholesteric transition. In contrast to Figure (14), the solid lines are drawn using the theoretical ρ^* and ρ_i values with no adjustable or fitted parameters.

terparticle correlations in both the isotropic and nematic phase [66], and indeed both phases are observed to have short range correlations. For the particular case of scattering from spheres there is a relationship between the scattering intensity $I(q)$ and the structure factor $S(q)$, which measures interparticle correlations $I(q) \propto F(q)S(q)$, with $F(q)$ the form factor, or scattering from a single particle and $q = 4\pi \sin(\theta)/\lambda$. However, this convenient intensity relation is not valid in general for rods, where the scattered intensity depends on the orientation of the rod axis with respect to the scattering vector. When the angular and spatial correlations are coupled, there is no direct way to separate the different correlations from the scattered intensity. The form factor of TMV, shown in Figure (18) is experimentally obtained by measuring the scattered intensity from a dilute suspension. Figure (19) shows the scattered intensity from a concentration series of isotropic samples of TMV in suspension at low ionic strength. This sample underwent an I - N transition near 30 mg/ml. The phase diagram in Fig. (4) suggests that this concentration corresponds to an ionic strength of about 3 mM. In turn, this implies an effective diameter about 3 - 4 times the hard
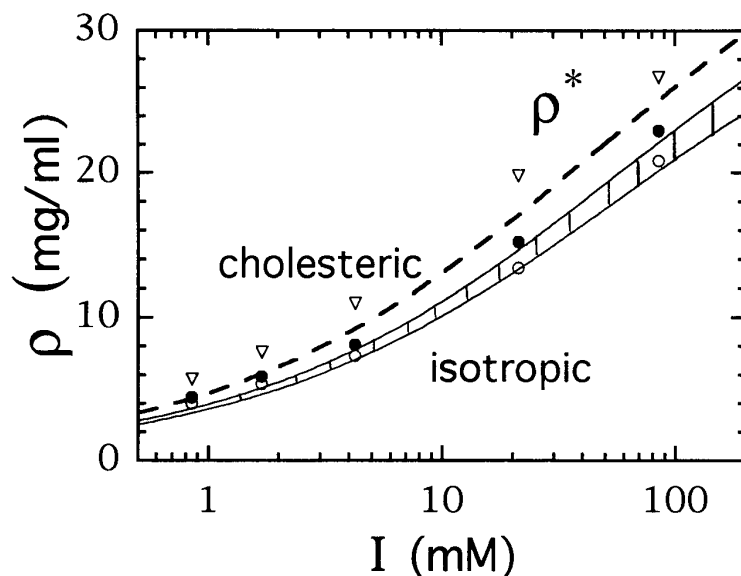
Figure 17. The experimental co-existence concentrations of the isotropic and cholesteric phases ρ_i (○), ρ_c (●) of fd, and the limit of stability (spinodal) of the isotropic phase ρ^* (▽), plotted at five ionic strengths. The calculated ρ_i and ρ_c (solid curves) are the same as in Figure (5), while the calculated ρ^* (dashed line) is from eq. (7).

diameter of TMV, which means that the rods are strongly repulsive. For lack of anything better to do, we divide the scattered intensity by the form factor and call the result the structure factor, also shown in Figure (19).

The structure factor has features at three length scales; low, intermediate, and high q. At low q, $S(q)$ is proportional to the isothermal compressibility $(\partial c/\partial\pi)$, and we observe that the suspension becomes less compressible with increasing concentration. Associated with the decrease in compressibility, there is an increase in $S(q)$ at intermediate q, and with increasing concentration first one peak and then two peaks develop. The location of the peak q_m is a measure of the average separation (R) between the central axes of the particles $q_m = 2\pi/R$, which for rods is *not* the center of mass as it is for spheres. From Figure (19) we find $R \sim 79$ nm. The width of the peak of the structure factor $\Delta q_m = 2\pi/\xi$ measures the spatial correlation length ξ of the rods. We see Δq_m narrows with increasing concentration, telling us that correlations are increasing. At the highest concentration close to the I - N transition, we find $\Delta q_m \sim 0.03$ nm^{-1} or $\xi \sim 210$ nm. The ratio $q_m/\Delta q_m = \xi/R$ is a measure of the number of particles in the spatial correlation length ξ and at the I - N transition this ratio
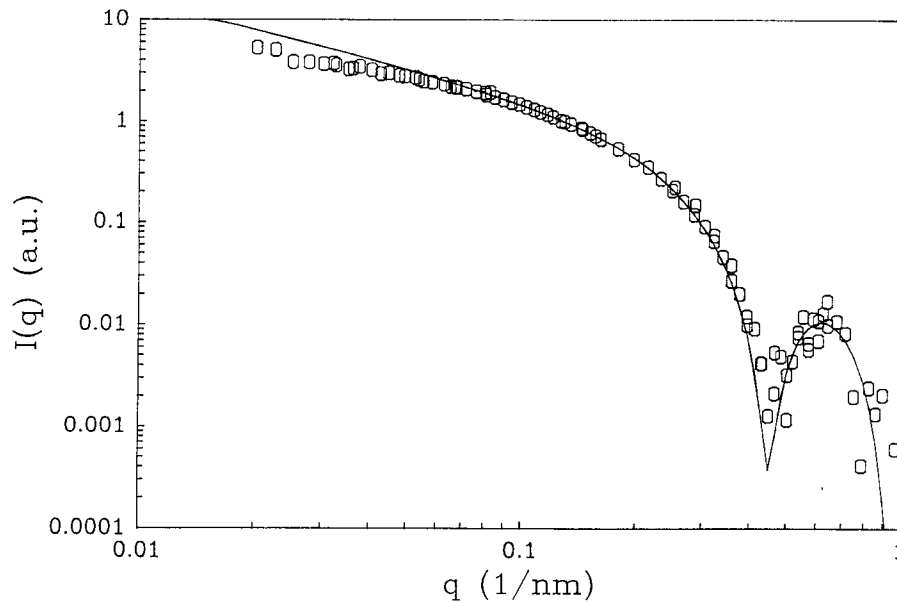
Figure 18. Calculated form factor of TMV from an isotropic suspension (-), compared to the experimentally measured scattered intensity from a sample of 11.2 mg/ml fd concentration and in 6 mM TRIS buffer at pH 8.

is about 3. We conclude that the spatial correlations are short - ranged and have similar magnitude to the angular correlations in the isotropic phase. Finally, at high q interparticle correlations vanish and $S(q) = 1$. These effects do not occur independently of each other. Once the rods are packed together with separations close to D_{eff} it becomes very difficult to further compress them, leading to the decrease in the osmotic compressibility and to the increase in local order, since in an energetic sense the rods are becoming close-packed.

6. Spatial correlations in the nematic phase of TMV

The scattered intensity from the nematic has a strong angular dependence, in contrast to the rotationally invariant isotropic phase. This is because at low resolution the virus particles can be approximated as a cylinder and their form factor is a series of thin rings (Bessel functions) in reciprocal space with the plane containing the rings perpendicular to the long axis of the cylinder. The thickness of the rings is inversely proportional to the
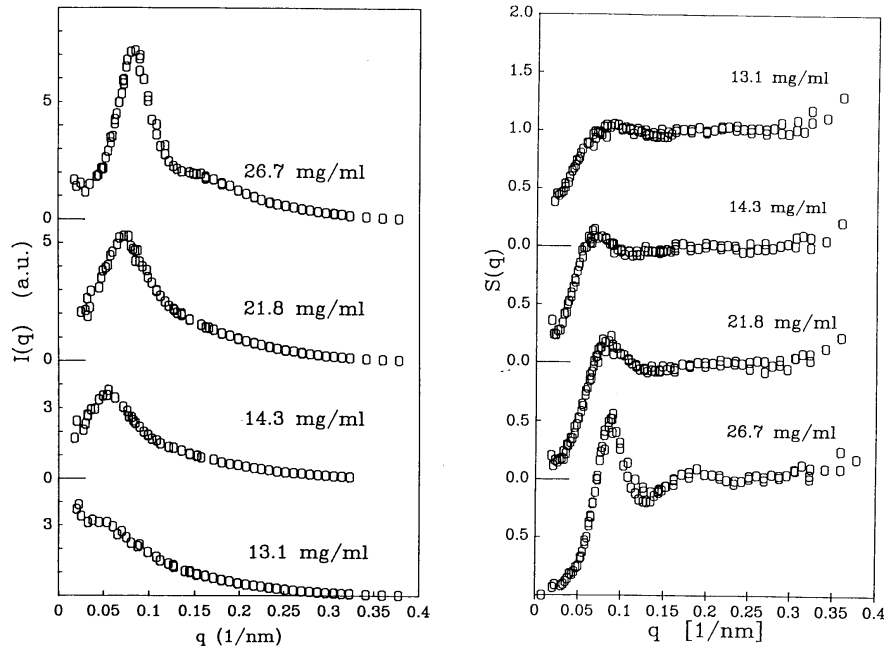
Figure 19. **(left)** The intensity $I(q)$ of neutron scattering from isotropic suspensions of TMV in distilled water. **(right)** The structure factor $S(q)$ is obtained by dividing the intensity data by the form factor of Fig. (18).

length of the cylinder and for our rotating anode x-ray scattering equipment and for the neutron scattering experiments, the finite thickness of the rings is unresolvable. Thus for a perfectly aligned nematic the scattering is confined to a line perpendicular to the nematic director and the intensity falls off as a Bessel function with increasing wavevector q.

In the nematic phase the orientational probability distribution is described by a Gaussian-like function with a narrow angular width. In the absence of interparticle interference, the scattered intensity from a nematic consists of a series of arcs centered on the beam with the maximum intensity concentrated along the equatorial scattering direction perpendicular to the nematic director. The angular distribution function is the central physical quantity in the Onsager model and has been measured in suspensions of TMV with x-ray scattering [8, 11]. Significant deviations in the shape of the angular distribution were found from the Onsager theory - the shape resembles a Gaussian more closely then the sharper peaked Onsager distribution. Comparisons with the Parsons - Lee theory [48] suggest that the
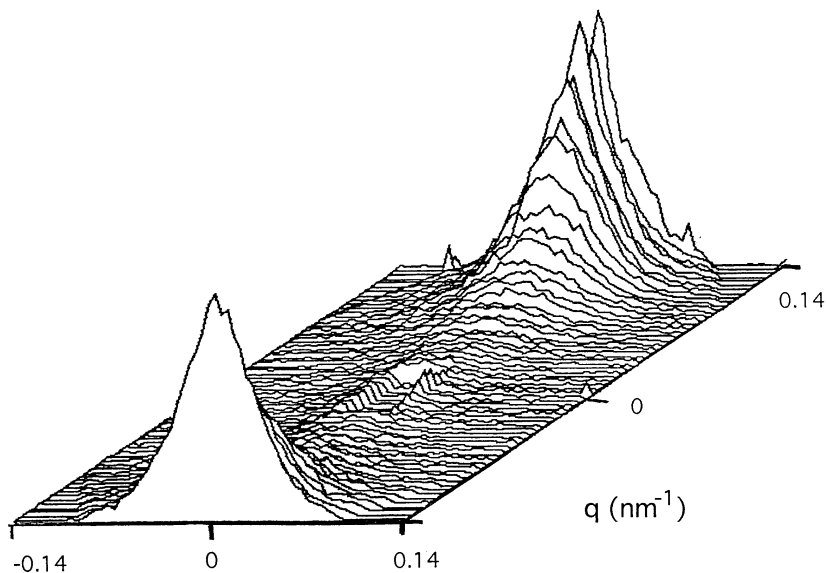
Figure 20. Low angle neutron scattering from aligned nematic TMV.

higher order virial terms are responsible for this deviation.

Fig. (20) shows the low angle scattered intensity from a magnetic field aligned nematic TMV sample of 74 mg/ml concentration at low ionic strength in H_2O. The data was taken on the D11 beam line of the Institut Laue-Langevin. The beam stop, or origin of reciprocal space is seen in the center of the two-dimensional plot as a rectangular depression and the scattering is dominated by two peaks. Scattering is strongly confined in the direction perpendicular to the nematic alignment direction. The width of the peaks at constant q is due to the angular distribution $f(\theta)$ of the orientation of the rods, and from this data, as well as measurements of the peaks at higher scattering angle arising from the form factor, we find that the order parameter $S = \int f(\theta)P_2(\theta)$ is 0.8.

It is notable that the scattered intensity in Fig. (20) does not at all resemble the form factor of TMV, which being a Bessel function, has its maximum at $q = 0$ and would gently decrease over the scattering angles shown. Instead we observe a strong peak at $q_m = 0.14$ nm^{-1}. The peak arises from interparticle interference and its radial width Δq_m is governed by the correlation length of the interacting particles. Fig. (21) shows the
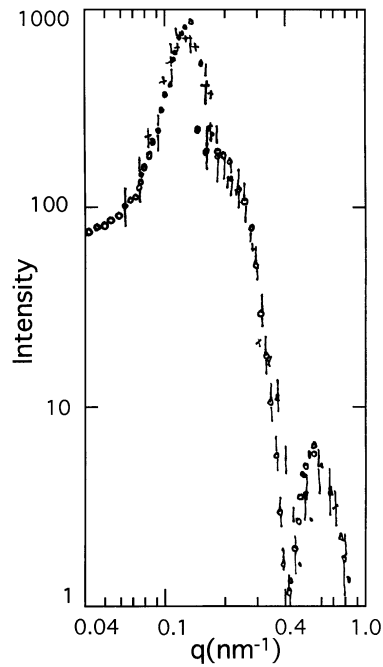
Figure 21. Radial averaged intensity from the nematic TMV of Fig. (20). The large peak at low q arises from interparticle interference and the smaller peak at high q is from the form factor as in Fig. (18).

radial averaged scattered intensity as a function of q. The decrease in intensity at low angles comes from the osmotic compressibility of the suspension, the first and largest peak arises from the interparticle interference, and the higher angle, weaker peak near 0.6 nm^{-1} is from the form factor of TMV shown in Fig. (18). The ratio $q_m/\Delta q_m \sim 3$ is approximately the number of particles in a correlation length. The number of particles in a correlation length in the nematic phase is nearly the same as in the isotropic phase, indicating that interparticle correlations are similar on each side of the isotropic - nematic transition.

Thorough x-ray scattering investigations of the angular distribution function and the interparticle correlations over the entire concentration range of both the nematic and smectic phases of TMV and fd are currently in progress at Brandeis.

7. Magnetic field induced isotropic - nematic phase transition

It has long been predicted that an external field, which orients the particles' long axis along the field, will induce a first order phase transition if the isotropic phase (I) is thermodynamically near the nematic phase (N) in the absence of the field [67, 68]. The basic intuition is that since the suspension is about to spontaneously align via a first order transition, a little nudge to increase the tendency to align will lower the transition concentration, c_i.

Due to the small size of the molecules, magnetic fields of order 1 mega-gauss (100 Tesla) are needed to observe the critical point [69], which is well above current obtainable DC field strengths. Only recently has the phase transition been observed using short bursts of high voltage a.c. fields [70]. However, due to the large $\Delta\chi$ of fd, fields of order 10 T will induce the phase transition. This is another example of how the large size of the colloid renders accessible experiments impossible for small molecule systems - in this case applying a field with energy of order kT per molecule.

To search for a field induced transition we built a 100x polarizing micro-scope to fit in a 20 tesla magnet and examined visually isotropic samples of fd in co-existence with the chiral nematic. The magnetic birefringence experiments were performed at the Francis Bitter National Magnet Labora-tory (FBNML) in a 20 tesla magnet equipped with a temperature stabilized holder, which was regulated at 22.0 C. Sample cells for all experiments had a 3 mm path length and were illuminated with a 1 mm diameter HeNe laser (633 nm) for birefringence measurements or white light for microscopy. Ini-tially when the field was swept from zero to 14 tesla in 30 sec., the intensity increased from dark to bright white, then uniform interference colors swept through the sample. After one minute small domains of several microns in size appeared uniformly throughout the sample forming an amorphous network and after 30 minutes, the droplets coarsened to order 20 microns. When the field was rapidly reduced to zero, the field induced network van-ished rapidly. The direct observation of droplet formation demonstrates that a first order phase transition has occurred, while the asymmetry in the times for build-up and decay of the droplets indicate that the dynamics of this process are very interesting. We set out to study the dynamics in detail by measuring the specific magnetic field induced birefringence $\Delta n/c$.

In our experiments $\Delta n/c$ was linear in field energy for small fields and for all concentrations as observed previously [61]. However, we observed a large non-linear increase in $\Delta n/c$ at high fields for concentrations in a narrow range of the I-N transition. Deviations from linear response were not observed previously [61] because the maximum magnetic field was 1 tesla, while at the FBNML we used fields up to 20 tesla, resulting in field energies a factor of 400 times greater. The non-linear increase, shown in Fig. (22)
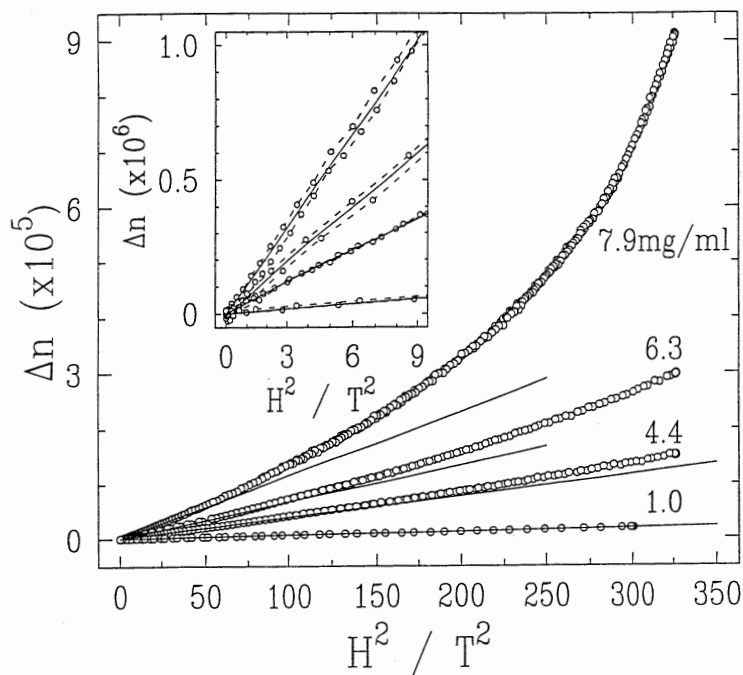
Figure 22. The magnetic field induced birefringence Δn, as a function of field squared H^2, at four representative fd concentrations. The open circles (o) are the experimental data, and the solid lines are linear fits of data at low fields (0-3T), except for the lowest concentration (1.0 mg/ml), for which the linear fit was applied to the entire field range. The upper window is a magnified display of the same data at low field. The open circles (o) connected by dotted lines with data below the solid lines were taken as the field increased and the data above taken as the field decreased. The birefringence is linear in H^2 at all concentrations in the weak field limit. The large nonlinear increase in Δn for the highest concentration is indicative of a field-induced phase transition [56]. All the samples were at Tris-Cl buffer at pH 7.5, with the ionic strength approximately 5 mM.

for freshly prepared *fd*, is indicative of field induced order, as opposed to a linear response, discussed previously, where the birefringence is due to the aligning of the existing correlation volumes along the field direction. At the highest fields, and for the highest concentrations we observed saturation of the birefringence, indicating the complete formation of a field induced nematic phase. These experiments are described in detail in ref. [56].

8. Cholesteric phase of fd

The molecules in a cholesteric phase are arranged locally as in a nematic phase, but there is a slight twist angle of constant sign between each

molecule. This results in precession of the director, illustrated in Fig. (23). The pitch p is the distance for the director to rotate 360 degrees. Viewed with a polarizing microscope a fd cholesteric sample has a texture that resembles a fingerprint [71] with a pattern of regularly spaced black lines separated by $p/2$. The Onsager theory of the nematic phase can be extended to calculate the elastic constants of the nematic [72], as well as the cholesteric pitch [73]. The minimum energy configuration of a macroscopic nematic is one with uniform alignment. The molecules are not all parallel, because the angular distribution function has a finite width, but the average direction of alignment, known as the director, points in one direction throughout the sample. A spatial variation in the director changes the angular distribution function from its ground state, raising the energy. The energy of the three possible distortions of the director field in a nematic, known as the twist, bend, and splay distortions has been calculated in the context of the Onsager theory [72].

A cholesteric can be thought of as being a nematic with a weak chiral perturbation. Straley [73] modeled a cholesteric as a suspension of hard screws, rather than hard rods. The excluded volume is reduced when two screws are oriented at an angle to each other because they can nest inside each others threads, as shown in Fig. (24). In Straley's model the pitch of a cholesteric results as a competition between the tendency for local twist, balanced against the cost of having a non-uniform director. The lowest energy configuration of a suspension of screws becomes one with a pure twist distortion, shown in Fig. (23). Straley predicted that the pitch is independent of concentration, because the energy cost of the twist elastic distortion and the energy gain produced by nesting the screws exactly compensate each other. The pitch was also found to be independent of concentration in a density functional calculation of hard twisted ellipsoids [74].

Odijk extended Straley's work to take into account flexibility, as well as reevaluating Straley's calculation [75]. Odijk finds that the pitch varies with concentration as

$$p \approx \Delta^{-1} P^{-4/3} D^{-5/3} c_p^{-5/3} \qquad (14)$$

with Δ the width of the thread, P the persistence length, D the inner radius of the screw, and c_p the concentration of persistence units given by $c_p = cL/P$.

The experimental situation is not clear, with some experiments supporting one theory, some the other. Studies on the polymer PBG show that $p \propto c^{-5/3}$ [76], while measurements on DNA show that p is independent of concentration [77]. The situation for fd is somewhere inbetween [71, 78]. In Fig. (25) the pitch is plotted as a function of concentration of fd in a 53 mM ionic strength buffer, pH 8. The data cover the entire concentration range
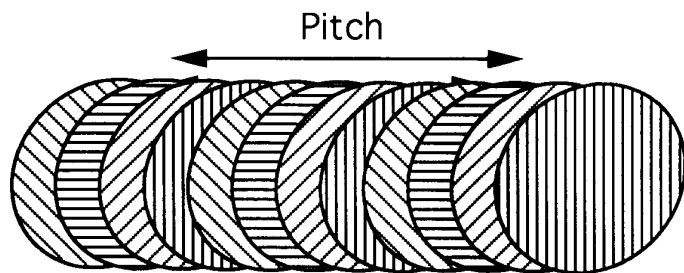
Figure 23. Schematic of the spatial variation of the director (represented as parallel lines) in a cholesteric phase. The pitch is the distance the director rotates 360 degrees.
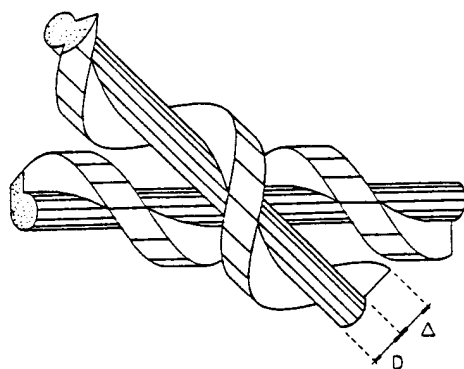

Figure 24. Geometry of two threaded rods. The upper rod may approach the lower most closely if its principal axis is rotated clockwise with respect to the axis of the lower. (After ref. [73])

of the cholesteric phase. At low concentration the isotropic phase transition occurs, and at the high end a smectic phase appears. The predicted power law $p \propto c^{-\alpha}$ with $\alpha = 5/3$ is observed for most of the concentration range. However, α is a function of ionic strength and α decreases systematically from $\alpha = 5/3$ at 64 mM ionic strength to $\alpha = 1.1$ at an ionic strength of 5 mM. If in eq. (14) we replace D with D_{eff}, our usual prescription for accounting for charge, we expect $\alpha = 5/3$ independent of ionic strength. This discrepancy suggests the need to reexamine the theories of the cholesteric phase and/or incorporate the effect of charge in a more basic way.

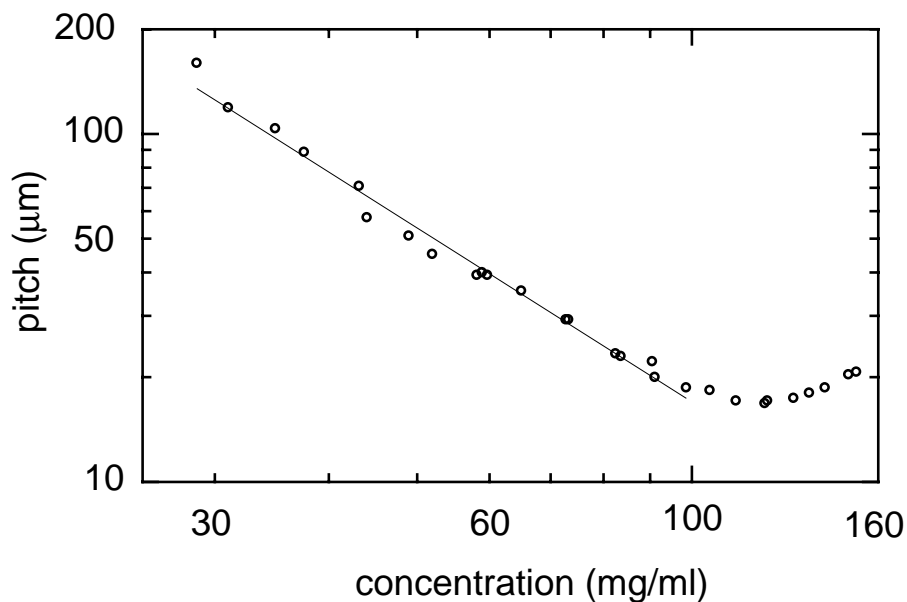We are currently measuring the twist elastic constant as a function of

Figure 25. A log - log plot of the pitch p as a function of fd concentration in a 53 mM ionic strength, pH 8 solution. The solid line is a fit to $p \propto c^{-\alpha}$ with $\alpha = 1.66$, in accord with the theory of Odijk [75]. At high concentration, smectic pre-transitional unwinding of the helix is seen.

ionic strength and fd concentration to more completely characterize the cholesteric phase. Initial studies of the twist elastic constant can be found in the thesis of Oldenbourg [78].

9. Smectic phase of fd and TMV

Visually, the most remarkable feature of the smectic phases of TMV and fd is that they are brilliantly iridescent [10, 12, 36, 71, 79]. This arises from the Bragg diffraction of light from the virus particles arranged in layers. The layer spacing is approximately equal to the particle length, which for both cases is of order the wavelength of light. In contrast, the separation of the particles in the plane of the layers is roughly in the range of 10 - 100 nm and x-rays or neutrons are needed to probe the structure on this length scale. Thus while the observance of iridescence demonstrates crystallinity in one-dimension, this observation alone is insufficient to differentiate between a crystal and a smectic. X-ray scattering studies [10, 80] revealed that TMV forms a smectic at high ionic strength, but at low ionic strengths the nematic phase directly transforms to a colloidal crystal. Recently, studies

at Brandeis have concluded that the TMV nematic - smectic transition is second order [81], in agreement with the hard rod simulations [5], and critical behavior for both the static divergence of scattered light and the dynamics of pre-smectic fluctuations have been observed [81].

Previous freeze fracture electron microscopy and optical microscopy studies have been made of fd smectics [71, 82], but were unable to present a consistent picture of its properties. In Figure (2) we mapped out the cholesteric - smectic (C-S) phase boundary of fd as a function of ionic strength. The agreement between the Khokhlov - Semenov theory of the isotropic - cholesteric transition with the experimental data of Figure (5) demonstrated that one can consider that the effect of ionic strength is to control the effective diameter of the particle. This allows us to introduce the concept of an effective volume fraction along the C - S phase boundary defined as $\phi_{\text{eff}} = c_s V_{\text{eff}}$ with c_S the number density at the C - S transition, $V_{\text{eff}} = \pi L (D_{\text{eff}}^{\text{nem}})^2/4$ with V_{eff} and $D_{\text{eff}}^{\text{nem}}$ the effective volume and diameter of the rods in the nematic phase. $D_{\text{eff}}^{\text{nem}}$ is calculated using the second virial coefficient in the Onsager theory: $D_{\text{eff}}^{\text{nem}} = D_{\text{eff}}^{\text{iso}}(1 + h\eta(f)/\rho(f))$ with h the twist parameter, and η and ρ functions of the angular distribution in the nematic phase [83]. The effective diameter increases as the rods become more ordered because the repulsive force for two parallel charged rods is greater than for crossed rods. The above definition of an effective diameter will be valid as long as the average angle $\sqrt{<\theta^2>}$ between particles in the nematic phase is greater than $D_{\text{eff}}^{\text{nem}}/L$ (see sec. 2.3 of ref [1]). We find that for a fd suspension with an order parameter of $S = 0.9$ [1] that $\sqrt{<\theta^2>} \sim 10 D_{\text{eff}}^{\text{nem}}/L$ for the largest value of $D_{\text{eff}}^{\text{nem}}$. Although the effective diameter diverges for long, strictly parallel charged rods, for fd with $S = 0.9$ with a twist constant $h < 0.15$, we find $D_{\text{eff}}^{\text{nem}} = 1.12 D_{\text{eff}}^{\text{iso}}$. Along the cholesteric - smectic (C - S) phase boundary we experimentally find that $\phi_{\text{eff}} = 0.75 \pm 0.05$, and this line of constant effective volume fraction is drawn in Figure (2).

This phase diagram is not athermal. We observed that a few fd samples were smectic in a 4° C refrigerator, but transformed into a cholesteric at room temperature. However, this temperature induced phase transition was only observed for samples of concentration very close to the C - S boundary.

We picture the smectic as consisting of layers of virus of uniform density separated by interlayer gaps where the density is lower. We model the density of ends of the virus particles in the gaps as having a Gaussian distribution, illustrated in Fig. (26),

$$\rho(z) = \rho_0 - \rho_1 \sum_n \delta(z - n\lambda) \otimes e^{-z^2/2\sigma^2} \tag{15}$$

with n the integers, ρ_0 and ρ_1 constants, and σ the gap width. Because the
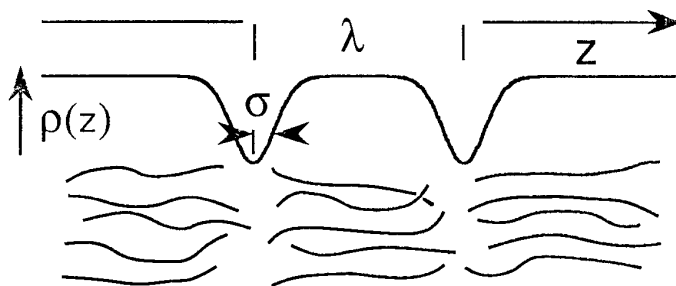
Figure 26. The bottom portion of this figure is a sketch of the distribution of the flexible fd molecules in the smectic phase. The upper portion is a plot of the density distribution of eq. (15), showing the density ρ as a function of distance z. The width of the gap between layers σ and the smectic layer spacing λ are indicated.

smectic is periodic in only one dimension, thermal fluctuations destroy long range order and the intensity of scattered light from the smectic layers will not have true Bragg peaks, but instead algebraic singularities. The intensity of the scattered light from $\rho(z)$ is

$$I(q_z) \propto e^{-q_z^2 \sigma^2} (q_z - q_0 m)^{\eta - 2} \tag{16}$$

with q_z the scattered wave vector, $q_0 = 2\pi/\lambda$ with λ the smectic periodicity, m the diffraction order, and η a function of the elastic moduli of the smectic phase and also increasing proportional to m^2 [84, 85]. We observed five Bragg diffraction peaks in light scattering measurements from aligned smectic samples with 479 nm light, but the peak widths did not increase with increasing m, indicating that η is much smaller than two. However, the integrated intensity of each peak did decrease according to eq. (16), and we determined that the gap between smectic layers has a width of $\sigma = 90 \pm 10$ nm and the smectic wavelength was $\lambda = 920 \pm 10$ nm. These values did not vary with ionic strength. The structure deduced from the model of eqs. (15) and (16) is sketched in Fig. 26.

As described in the previous section, we measured the cholesteric pitch as a function of concentration over the entire cholesteric phase for several ionic strengths. With increasing concentration the pitch initially decreases as $c^{-\alpha}$, with α a function of ionic strength, decreasing systematically with increasing ionic strength. The data for one ionic strength is shown in Fig. (25). In this case, when the fd concentration is increased above 100 mg/ml the cholesteric helix begins to unwind and the pitch increases until
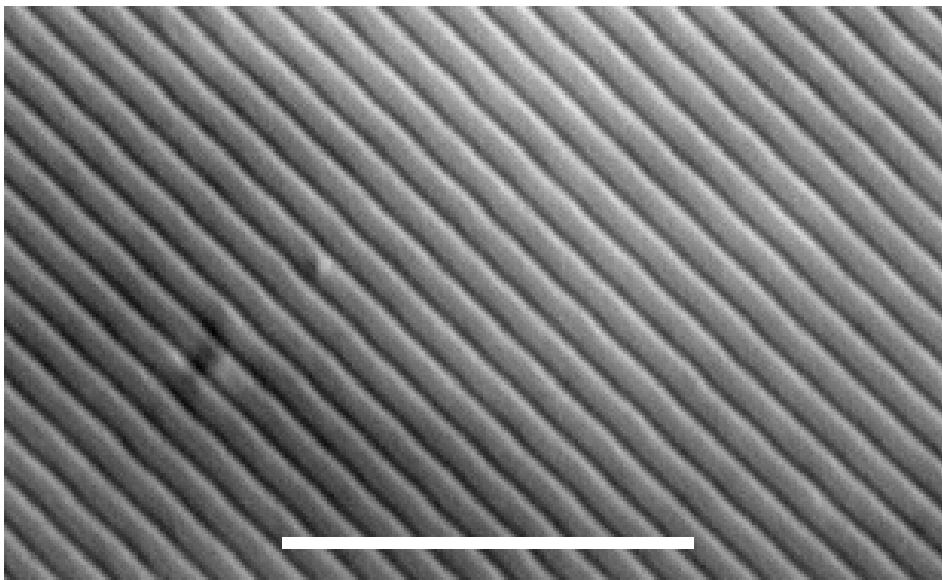
Figure 27. DIC optical micrograph of the fd smectic. The high contrast black- white lines are the gaps between smectic layers. The particles lie in the plane of the photo and are oriented perpendicular to the smectic planes. The smectic periodicity is 0.92 μm and the white bar is 10 μm.

150 mg/ml when the cholesteric - smectic phase transition occurs. This unwinding of the helix occurred for all samples when the concentration was within 10% of the smectic phase. In a second order C-S phase transition, the pitch would diverge continuously. Instead, we observe a slight increase in pitch followed by abrupt unwinding at the smectic phase boundary. We also note that there was no indication of pre-transitional smectic density fluctuations in light scattering measurements.

In general, if one can observe several diffraction orders with light, then it is possible to directly image the smectic layers with an optical microscope. A Differential Interference Contrast (DIC), video enhanced light microscope photograph of the smectic is shown in Fig. (27). The spatial resolution and depth of field is 0.2 μm [86]. The fd molecules are lying in the plane of the photo, oriented perpendicular to the dark bands, which are the gaps between the layers. Thermotropics are modeled as having a sinusoidal density modulation and show only one Bragg peak. In contrast, the smectic layers in Fig. (27) have a square-wave like density modulation, consistent with our observation of five diffraction orders, and consistent with the hard rod models.

The textures and defects possible in smectic phases include a wide variety depending on the relative roles of dislocations and disclinations. In the case of either externally imposed deformations or spontaneous cholesteric twist, the response of the smectic is governed by relative values of elastic moduli for the several first and second order elastic deformation terms in the free energy. Thus determining the defect textures is of great value in understanding the nature of the smectic ordering. A smectic resists the twist deformation because it destroys the layering, thus defects must be introduced when such a deformation is imposed. Under a twist strain, a smectic can respond by either accommodating the twist all at once by locally melting the smectic (analogous to a normal-Type I superconductor transition induced by a magnetic field), or by introducing a periodic array of defects and distributing the twist in discrete increments throughout the sample (analogous to the Abrikosov flux lattice in a Type II). Which behavior is observed depends on the relative cost of creating a smectic - nematic interface versus the cost of producing screw dislocations.

Shown in Fig. (28) are video enhanced DIC micrographs of textures in a fd smectic with the layers oriented normal to the slides (the "bookshelf" geometry), which is uniformly twisted between the top and bottom slides that contain it. In the superconducting analogy, this is equivalent to imposing a magnetic field on a superconductor. The spatial resolution and depth of field of the images are 0.2 μm. With serial images at different depths in a sample, we can map out the detailed three dimensional spatial configuration of the smectic layers, and Fig. (28) shows a series of images separated in depth by 0.5 μm. The imposed twist is accommodated in the smectic by taking the form of a series of regularly spaced blocks of smectics with a constant angle of rotation between adjacent blocks [87], as illustrated in Fig 29. Although only three blocks are shown in Figs. 28a, 28c, and 28e, this pattern persisted throughout the 5 μm thick sample. In between each block are expected a series of regularly spaced twist grain boundaries (TGB). However, the structure in the plane of the screw dislocations cannot be seen because of the finite depth of field of the microscope. Instead, when focused at the interface between smectic blocks we observe a Moiré pattern from the blocks above and below the focus plane (Figs. 28b and 28d). This sets an upper limit on the thickness of the grain boundary of less than 0.2 μm and establishes that the blocks rotate in discrete amounts, as expected for the TGB texture.

We now compare the above experimental results of the smectic phase of the semi-flexible molecule fd with the results from simulations, theory, and experiment from either hard or charged rigid particles. We saw in the discussion of Fig. (2) that by considering the effect of ionic strength as merely changing the effective diameter of fd, we were led to conclude that
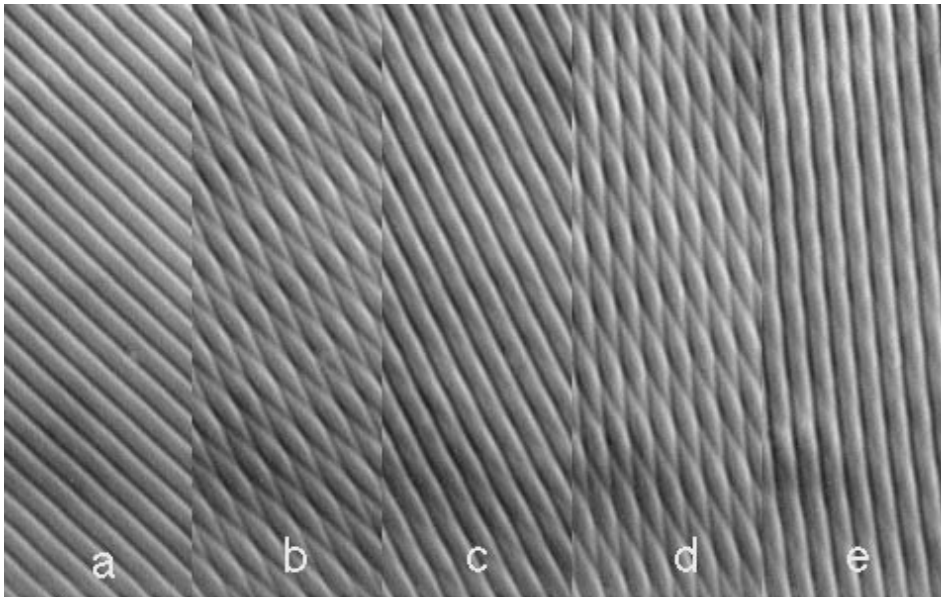
158

Figure 28. DIC photograph of a strain-induced TGB texture. Montage of five images, each displaced vertically by 0.5 μm. The resolution in the plane of the photo is 0.2 μm, and the depth of field is also 0.2 μm. In (a), (c), and (e) smectic blocks are observed in the bookshelf geometry with the fd molecules in the plane of the photo and aligned perpendicular to the dark lines, which define the smectic layer spacing of 920 nm. The texture in (b) and (d) is a Moiré pattern from the two adjacent images and is generated because of the 0.2 μm depth of field of the microscope.

the volume fraction at the cholesteric - smectic transition was a constant $\phi_{\text{eff}} = 0.75 \pm 0.05$, even though L/D_{eff} increases from about 30 to 70 as the ionic strength varies from 4 - 65 mM. The theories and simulations show that the volume fraction at the smectic transition initially decreases with increasing L/D, but becomes constant above $L/D > 10$ [89], thus the independence of ϕ_{eff} on L/D_{eff} is expected. However, ϕ_{eff} is substantially higher than observed in simulations or theory for rigid and hard particles, for which $\phi = 0.4 - 0.5$ is found [1, 89]. We conclude that introducing flexibility acts to suppress the phase transition.

As discussed previously, the fd liquid crystal is not athermal because the degree of flexibility is temperature dependent. In Fig. (9) we showed that the persistence length P has a non-monotonic temperature dependence, first decreasing from 2.45μm to 2.15μm as the temperature increases from 4 to 35° C. As mentioned above, a smectic sample of concentration close to the cholesteric phase boundary would undergo a smectic - cholesteric
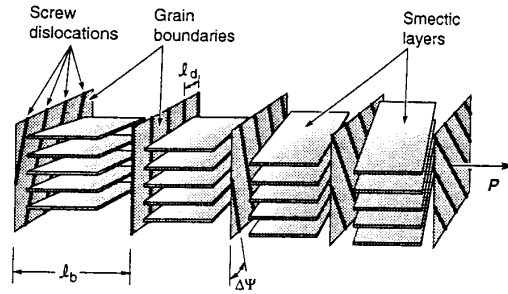
Figure 29. Schematic representation of the TGB model of the SmA phase. Blocks of SmA layers of spacing d are separated by regularly spaced twist grain boundaries separated by a distance l_b. The distance between screw dislocations within a grain boundary is l_d. The angles of the normal to the smectic planes separated by a grain boundary differ by $\Delta\Psi \sim d/l_d$. The molecular director lies in planes perpendicular to the pitch axis, P. The average configuration of the director in the TGB model is very similar to that of the cholesteric phase. (Figure after ref [88]).

transition upon warming from 4 to 20° C. This temperature change induces about a 10% decrease in the persistence length, and is consistent with the conclusion that increasing flexibility suppresses the C - S transition.

The light scattering and optical microscopy studies revealed that the ratio of smectic periodicity to fd contour length was $\lambda/L = 1.05$. Theory and simulations of hard cylinders have a much larger value $\lambda/L = 1.4$, while experiments on TMV, a rigid, but charged cylinder has $\lambda/L = 1.1 - 1.2$. The shape of the ends of the particles has a strong effect on the layer spacing and volume fraction of the smectic phase. Rounding the ends of hard, rigid cylinders both raises ϕ and lowers λ/L [89], and in the case of an ellipsoid of revolution the smectic phase is completely suppressed [90]. One can imagine that the effect of charge is to "round" the edges of TMV and fd, thus accounting for the lowered values of λ/L compared to the hard particles. But since λ/L is even smaller for fd than for TMV, we conclude that flexibility lowers λ/L compared to rigid particles.

The two observations of weak pre-transitional unwinding of the cholesteric helix and the undetectable pre-transitional fluctuations in the smectic order parameter using light scattering, coupled with the observations of the discontinuous tremendous increase in the scattered light intensity and sudden unwinding of the cholesteric helix at the cholesteric - smectic phase boundary indicate that the C - S transition is first order. This is in contrast to both the simulations of hard, rigid particles and the experiments on TMV where the nematic - smectic transition is second order. We conclude

that the effect of flexibility is to drive the second order nematic - smectic transition to be first order.

10. Conclusions

Suspensions of virus particles have proven to be model systems for exploring liquid crystalline properties. They come in a variety of shapes and sizes and are amenable to modification using molecular engineering techniques. These virus systems offer numerous examples of how the colloidal dimensions of the particles offer unique experimental opportunities, not available to small molecule systems. These include the magnetic field induced isotropic - nematic transition in fd, determination of the dynamical exponent of pre-smectic density fluctuations in TMV using dynamic light scattering, and direct microscopic observation of smectic layering. On one hand the viruses have been proving grounds for testing theories. The isotropic - nematic transition in fd suspensions has been shown to be quantitatively described by extensions of the Onsager theory of charged, rigid particles that account for the flexibility of fd. On the other hand, the virus systems raise many fundamental questions. What is the molecular origin of the cholesteric order in virus suspensions? TMV, pf1, and fd have chiral symmetry in that they are composed of helical arrays of proteins, yet why does fd form a cholesteric while both TMV and pf1 form a nematic? A second fundamental question concerns the role of flexibility in liquid crystals for which there have been neither experiment, simulation, or theory: How flexible can a polymer be and still form a smectic? How does flexibility effect the order of the nematic - smectic transition? We believe that these model virus systems will be of use in exploring these questions, but clearly there is also the need for the parallel development of both theories and simulations.

References

1. Vroege, G.J. and Lekkerkerker, H.N.W. (1992) Phase transitions in lyotropic colloidal and polymer liquid crystals. *Repts. on Prog. Phys.*, **8**,1241.
2. Allen, M.P., Evans, G.T., Frenkel, D. and Mulder, B.M. (1993) Hard convex body fluids. In I. Prigogine and S. A. Rice, editors, *Advances in Chem. Phys., vol. LXXXVI*, pages 1 − 166.
3. Tarazona, P. (1993) Theories of phase behaviour and phase transitions in liquid crystals. *Phil. Trans. R. Soc. Lond. A*, **344**,307.
4. Stroobants, A., Lekkerkerker, H.N.W. and Frenkel, D. (1986) Evidence for smectic order in a fluid of hard parallel spherocylinders. *Phys. Rev. Lett.*, **57**,1452.
5. Stroobants, A., Lekkerkerker, H.N.W. and Frenkel, D. (1987) Evidence of one-, two-, and three-dimensional order in a system of hard parallel spherocylinders. *Phys. Rev. A*, **36**,2929.
6. Frenkel, D. (1992) Computer simulations of phase transitions in liquid crystals. In S. Martellucci and A. N. Chester, editors, *Phase Transitions in Liquid Crystals*, pages 67 − 95. Plenum Press.
7. Allen, M.P. (1993) Simulations using hard particles. *Phil. Trans. R. Soc. Lond. A*, **344**,323.
8. Oldenbourg, R., Wen, X., Meyer, R.B. and Caspar, D.L.D. (1988) Orientational distribution function in nematic Tobacco Mosaic Virus liquid crystals measured by x-ray diffraction. *Phys. Rev. Lett.*, **61**,1851.
9. Fraden, S., Maret, G. and Caspar, D.L.D. (1993) Angular correlations and the isotropic-nematic phase transition in suspensions of Tobacco Mosaic Virus. *Phys. Rev. E*, **48**,2816.
10. Wen, X., Meyer, R.B. and Caspar, D.L.D. (1989) Observation of smectic-A ordering in a solution of rigid-rod-like particles. *Phys. Rev. Lett.*, **63**,2760.
11. Meyer, R.B. (1990) Ordered phases in colloidal suspensions of Tobacco Mosaic Virus. In A. Onuki and K. Kawasaki, editors, *Dynamics and Patterns in Complex Fluids*, page 62. Springer Proceedings in Physics, vol. **52**, Springer-Verlag.
12. Wetter, C. (1985) Die flüssigkristalle des tabakmosaikvirus. *Biologie in unserer Zeit*, **3**,81 − 89.
13. Hansen, J.P. and McDonald, I.R. (1986) *Theory of Simple Liquids*. Academic, London, second edition.
14. Israelachvili, J.N. and Ninham, B.W. (1977) Intermolecular forces - the long and short of it. *J. of Coll. and Int. Sci.*, **58**,14.
15. Forsyth, P.A., Jr., Marčelja, S., Mitchell, D.J. and Ninham, B.W. (1978) Ordering in colloidal systems. *Adv. in Coll. and Int. Sci.*, **9**,37.
16. Lekkerkerker, H.N.W. (1992) Disorder-to-order phase transitions in concentrated colloidal dispersions. In S.-H. Chen *et. al.*, editor, *Structure and Dynamics of Strongly Interacting Colloids and Supramolecular Aggregates in Solution*, page 97. Kluwer Academic Publishers.
17. Bernal, J.D. and Fankuchen, I. (1941) X-ray and crystallographic studies of plant virus. *J. Gen. Physiol.*, **25**,111 − 165.

18. Glucksman, M.J., Bhattacharjee, S. and Makowski, L. (1992) Three-dimensional structure of a cloning vector. *J. Mol. Biol.*, **226**,455 − 470.

19. Klug, A. and Caspar, D.L.D. (1960) The structure of small viruses. *Adv. in Virus Research*, **7**,225.

20. Loh, E., Ralston, E. and Schumaker, V.N. (1979) Quasielastic light scattering from solutions of filamentous viruses. I. experimental. *Biopolymers*, **18**,2549.

21. Loh, E. (1979) Quasielastic light scattering from solutions of filamentous viruses. II. Comparison between theories and experiments. *Biopolymers*, **18**,2569.

22. Lauffer, M.A. (1938) Optical properties of solutions of Tobacco Mosaic Virus protein. *J. Phys. Chem.*, **42**,935.

23. Gray, C.W., Brown, R.S. and Marvin, D.A. (1981) Adsorption complex of filamentous fd virus. *J. Mol. Biol.*, **146**,621–627.

24. Day, L.A., Marzec, C.J., Reisberg, S.A. and Casadevall, A. (1988) DNA packing in filamentous bacteriophages. *Ann. Rev. Biophys. Chem.*, **17**,509.

25. Maeda, T. and Fujime, S. (1985) Dynamic light-scattering study of suspensions of fd virus. Application of a theory of the light-scattering spectrum of weakly bending filaments. *Macromolecules*, **18**,2430.

26. Song, L., Kim, U-S, Wilcoxon, J. and Schurr, J.M. (1991) Dynamic light scattering from weakly bending rods: Estimation of the dynamic bending rigidity of the m13 virus. *Biopolymers*, **31**,547.

27. Zimmermann, K., Hagedorn, J., Heuck, C.C., Hinrichsen, M. and Ludwig, J. (1986) The ionic properties of the filamentous bacteriophages pf1 and fd. *J. Biol. Chem.*, **261**,1653.

28. Herrmann, R., Neugebauer, K., Pirkl, E., Zentgraf, H. and Schaller, H. (1980) Conversion of bacteriophage fd into an efficient single-stranded DNA vector system. *Molec. gen. Genet.*, **177**,231–242.

29. Doedtker, H. and Simmons, N.S. (1958) The preparation and characterization of essentially uniform TMV particles. *J. Am. Chem. Soc.*, **80**,2550.

30. Newman, J., Swinney, H.L. and Day, L.A. (1977) Hydrodynamic properties and structure of fd virus. *J. Mol. Biol.*, **116**,593.

31. O'Konski, C.T., Yoshioda, K. and Orttung, W.H. (1959) Electric properties of macromolecules. IV. Determination of electric and optical parameters from saturation of electric birefringence in solutions. *J. Amer. Chem. Soc.*, **63**,1558.

32. Torbet, J. and Maret, G. (1981) High-field magnetic birefringence study of the structure of rodlike phages pf1 and fd in solution. *Biopolymers*, **20**,2657.

33. Parsegian, V.A. and Brenner, S.L. (1976) The role of long range forces in ordered arrays of TMV. *Nature*, **259**,632.

34. Newman, J. and Swinney, H.L. (1976) Length and dipole moment of TMV by laser signal-averaging transient electric birefringence. *Biopolymers*, **15**,301.

35. Wilcoxon, J. and Schurr, J.M. (1983) Dynamic light scattering from thin rigid rods: Anisotropy of translational diffusion of TMV. *Biopolymers*, **22**,849.

36. Kreibig, U. and Wetter, C. (1980) Light diffraction of *in vitro* crystals of six tobacco Mosaic Viruses. *Z. Naturforsch.*, **35 C**,750.

37. Sambrook, J., Fritsch, E.F. and Maniatis, T. (1989) *Molecular Cloning: A Laboratory Manual*, volume 1, chapter 4: Single-stranded, Filamentous Bacteriophage Vectors. Cold Spring Harbor Laboratory Press, second edition.

38. Griess, G.A., Moreno, E.T., Herrmann, R. and Serwer, P. (1990) The sieving of rod-shaped viruses during agarose gel electrophoresis. I. Comparison with the sieving of spheres. *Biopolymers*, **29**,1277.

39. Onsager, L. (1949) The effects of shape on the interaction of colloidal particles. *Ann. N.Y. Acad. Sci.*, **51**,627.

40. Stroobants, A., Lekkerkerker, H.N.W. and Odijk, Th. (1986) Effect of electrostatic interaction on the liquid crystal phase transition in solutions of rodlike polyelectrolytes. *Macromolecules*, **19**,2232.

41. Odijk, Th. (1986) Theory of lyotropic polymer liquid crystals. *Macromolecules*,

19,2313.

42. Straley, J.P. (1973) Third virial coeffiecient for the gas of long rods. *Mol. Cryst. Liquid Cryst.*, **24**,7.

43. Frenkel, D. and Mulder, B.M. (1985) The hard ellipsoid-of-revolution fluid. I. Monte carlo simulations. *Mol. Phys.*, **55**,1171.

44. Bawden, F.C., Pirie, N.W., Bernal, J.D. and Fankuchen, I. (1936) Liquid crystalline substances from virus infected plants. *Nature*, **138**,1051.

45. Tang, J. and Fraden, S. Isotropic - cholesteric phase transition in colloidal suspensions of filamentous bacteriophage fd. *Liquid Crystals*. To be published.

46. Fraden, S., Hurd, A.J., Meyer, R.B., Cahoon, M. and Caspar, D.L.D. (1985) Magnetic field induced alignment and instabilities in ordered colloids of Tobacco Mosaic Virus. *J. de Physique*, **C3**,85 − 113.

47. Tang, J. and Fraden, S. Temperature dependence of the flexibility of fd: Behavior of the isotropic - cholesteric phase boundary and magnetic birefringence. *Biopolymers*. Submitted for publication.

48. Lee, S-D. (1987) A numerical investigation of nematic ordering based on a simple hard-rod model. *J. Chem. Phys.*, **87**,4972.

49. deGennes, P.G. and Prost, J. (1993) *The Physics of Liquid Crystals*. Oxford Science, second edition.

50. Khokhlov, A.R. and Semenov, A.N. (1982) Liquid-crystalline ordering in the solution of partially flexible macromolecules. *Physica*, **112A**,605.

51. Semenov, A.N. and Khokhlov, A.R. (1988) Statistical physics of liquid-crystalline polymers. *Sov. Phys. Usp.*, **31**,988–1014.

52. Chen, Z.Y. (1993) Nematic ordering in semiflexible polymer chains. *Macromolecules*, **26**,3419.

53. Vroege, G.J. (1989) The isotropic-nematic phase transition and other properties of a solution of semiflexible polyelectrolytes. *J. Chem. Phys.*, **90**,4560.

54. Vroege, G.J. and Lekkerkerker, H.N.W. (1993) Theory of the isotropic-nematic-nematic phase separation for a solution of bidisperse rodlike particles. *J. Phys. Chem.*, **97**,3601.

55. Tang, J. (1994) *Isotropic-Cholesteric Co-Existence and Magnetic-Field-Induced Isotropic-Nematic Transition of Filamentous Bacteriophage fd*. PhD thesis, Brandeis University.

56. Tang, J. and Fraden, S. (1993) Magnetic field induced isotropic - nematic phase transition in a colloidal suspension. *Phys. Rev. Lett.*, **71**,3509.

57. Maret, G. and Dransfeld, K. (1985) High magnetic fields in biology. In F. Herlach, editor, *Strong and Ultrastrong Magnetic Fields and Their Applications*. Springer-Verlag.

58. Straley, J.P. (1973) The gas of long rods as a model for lyotropic liquid crystals. *Mol. Cryst. Liquid Cryst.*, **22**,333.

59. Frattini, P.L. and Fuller, G.G. (1984) A note on phase-modulated flow birefringence: A promising rheo-optical method. *J. Rheol.*, **28**,61.

60. Fuller, G.G. (1990) Optical rheometry. *Annu. Rev. Fluid Mech.*, **22**,387.

61. Nakamura, H. and Okano, K. (1983) Pretransitional phenomena in the isotropic phase of a lyotropic liquid crystal of baterial virus fd. *Phys. Rev. Lett.*, **50**,186.

62. Photinos, P., Rosenblatt, C., Schuster, T.M. and Saupe, A. (1987) Magnetic birefringence study of isotropic suspensions of tobacco mosaic virus. *J. Chem. Phys.*, **87**,6740.

63. Frenkel, D. (1988) Structure of hard-core models for liquid crystals. *J. Phys. Chem.*, **92**,3280.

64. Allen, M.P. and Frenkel, D. (1987) Observation of dynamical precursors of the isotropic - nematic transition by computer simulation. *Phys. Rev. Lett.*, **58**,1748.

65. Frenkel, D. Personnel communication.

66. Maier, E.E., Krause, R., Deggelmann, M., Hagenbuchle, M., Weber, R. and Fraden, S. (1992) Liquidlike order of charged rodlike particle solutions. *Macromolecules*,

25,1125 − 1133.

67. Hanus, J. (1969) Effect of the molecular interaction between anisotropic molecules on the optical kerr effect. Field-induced phase transition. *Phys. Rev.*, **178**,420.

68. Khokhlov, A.R. and Semenov, A.N. (1982) Influence of external field on the liquid-crystalline ordering in solutions of stiff-chain macromolecules. *Macromolecules*, **15**,1272.

69. Hornreich, R.M (1985) Landau theory of the isotropic-nematic critical point. *Phys. Lett.*, **109A**,232.

70. Lelidis, I. and Durand, G. (1993) Electric-field-induced isotropic-nematic phase transition. *Phys. Rev. E*, **48**,3822.

71. Lapointe, J. and Marvin, D.A. (1973) Filamentous bacterial viruses VIII. Liquid crystals of fd. *Mol. Crys. Liq. Crys.*, **19**,269.

72. Straley, J.P. (1973) Frank elastic constants of the hard-rod liquid crystal. *Phys. Rev. A*, **8**,2181.

73. Straley, J.P. (1976) Theory of piezoelectricity in nematic liquid crystals, and of the cholesteric ordering. *Phys. Rev. A*, **14**,1835 − 1841.

74. Evans, G.T. (1992) Hard body model for chiral nematic liquid crystals. *Mol. Phys.*, **77**,969.

75. Odijk, Th. (1987) Pitch of a polymer cholesteric. *J. Phys. Chem.*, **91**,6060 − 6062.

76. DuPre, D.B. and Duke, R.W. (1975) Temperature, concentration, and molecular weight dependence of the twist elastic constant of cholesteric poly-γ-benzyl-L-gluamate. *J. Chem. Phys.*, **63**,143.

77. Van Winkle, D.H., Davidson, M.W., Chen, W.X. and Rill, R.L. (1990) Cholesteric helical pitch of near persistence length DNA. *Macromolecules*, **23**,4140 − 4148.

78. Oldenbourg, R. (1981) *Elastische und quasielastische Lichtstreuung an magnetisch ausgerichteten polyelektrolytischen Stäbchen.* PhD thesis, Universität Konstanz, Germany.

79. Oster, G. (1950) Two-phase formation in solutions of Tobacco Mosaic Virus and the problem of long range forces. *J. Gen. Physiol.*, **33**,445.

80. Fraden, S., Caspar D.L.D. and Phillips, W.C. (1982) X-ray diffraction studies of colloid crystalline TMV. *Biophys. J.*, **37a**,94a.

81. Wang, J.H., Lonberg, F., Ao, X. and Meyer, R.B. (1994) Light scattering studies of a nematic to smectic-A phase transition in rigid rod polymer solutions. In A. Teramoto, M. Kobayashi, and T. Norisuje, editors, *Ordering in Macromolecular Systems.* Springer-Verlag.

82. Booy, F.P. and Fowler, A.G. (1985) Cryo-electron microscopy reveals macromolecular organization within biological liquid crystals seen in the polarizing microscope. *Int. J. Biol. Macromol.*, **7**,327 − 335.

83. The definitions of h, ρ, and η are in sec. 2.6 of ref. [1]. The functions ρ and η are tabulated in ref. [40], and the values for h and $D_{\text{eff}}^{\text{iso}}$ for fd are taken from ref. [45].

84. Caille, A. (1972) *C. R. Hebd. Acad. Scien. Ser. B*, **274**,891.

85. Gunther, L., Imry, Y. and Lajzerowis, J. (1980) *Phys. Rev. A*, **22**,1733.

86. Inoue, S. (1989) Imaging of unresolved objects, superresolution,.. *Methods in Cell Biology*, **30**,85.

87. Renn, S.R. and Lubensky, T.C. (1988) Abrikosov dislocation lattice in a model of the cholesteric-to-smectic-A transition. *Phys. Rev. A*, **38**,2132.

88. Ihn, K.J., Zasadzinski, J.A.N., Pindak, R., Slaney, A.J. and Goodby, J. (1992) Observations of the liquid crystal analog of the Abrikosov phase. *Science*, **258**,275−278.

89. Evans, G.T. (1992) Liquid crystal smectic-A phases and issues of geometry. *Mol. Phys.*, **76**,1359.

90. Mulder, B. (1987) Density-functional approach to smectic order in an aligned hard-rod fluid. *Phys. Rev. A*, **35**,3095.